CENOZOIC TECTONIC EVOLUTION OF THE BASIN AND RANGE PROVINCE IN NORTHWESTERN NEVADA

JOSEPH P. COLGAN*[†], TREVOR A. DUMITRU*, PETER W. REINERS**, JOSEPH L. WOODEN***, and ELIZABETH L. MILLER*

ABSTRACT. A regional synthesis of new and existing geologic and thermochronologic data document late Cretaceous - early Cenozoic regional erosion, Oligocene - Miocene volcanism, and subsequent late Miocene extension of the Basin and Range Province in northwestern Nevada and northeastern California. Across an ~220-km-wide region between the Santa Rosa and Warner Ranges, conformable sequences of 35 to 15 Ma volcanic rocks are cut by only a single generation of high-angle normal faults that accommodated ~23 km of total east-west extension (~12%). Fission-track, (U-Th)/He, geologic, and structural data from the Pine Forest Range show that faulting there began at 11 to 12 Ma, progressed at a relatively constant rate until at least 3 Ma, and has continued until near the present time. Extension in the Santa Rosa Range to the east took place during the same interval, although the post-6 Ma part of this history is less well constrained. Less complete constraints from adjacent ranges permit a similar timing for faulting, and we infer that extensional faulting in northwestern Nevada began everywhere at 12 Ma and has continued up to the present. Faulting in the Warner Range in northeastern California can only be constrained to have begun between 14 and 3 Ma, but may represent westward migration of Basin and Range extension during the Pliocene. Compared to the many parts of the Basin and Range in central and southern Nevada, extension in northwestern Nevada began more recently, is of lesser total magnitude, and was accommodated entirely by high-angle normal faults. Fission-track data document Late Cretaceous unroofing of Cretaceous (115 – 100 Ma) granitic basement rocks in northwestern Nevada, followed by a long period of relative tectonic quiescence that persisted through Oligocene and Miocene volcanism until the onset of Basin and Range extension at ~12 Ma. The low magnitude of extension (12%) and early Tertiary stability suggest that the modern ~31 km thick crust in northwestern Nevada was only slightly thicker (~35 km) prior to extension at 12 Ma, and was no thicker than ~38 km in the Late Cretaceous. This stands in contrast to other parts of the Basin and Range, where the crust was thickened to at least 45 to 50 km by Cretaceous thrusting and subsequently thinned to ~30 km by large magnitude (>50%) extension.

INTRODUCTION

Detailed reconstructions of the timing and magnitude of Cenozoic faulting in the Basin and Range Province are important for understanding both the processes of continental extension and the pre-extensional structural and thermal conditions that led to large-scale extension of the western United States. Information on the timing and magnitude of extensional faulting remains sparse in many areas, particularly the northwestern part of the province in northwestern Nevada and northeastern California (fig. 1). This region spans the northwestern boundary of the Basin and Range Province and differs in several important aspects from the main part of the Basin and Range in central Nevada.

In central Nevada (at roughly lat 38 – 40°, fig. 1), modern basin-range topography began forming during a widespread episode of major normal fault slip ca. 19 to 14 Ma

*Department of Geological and Environmental Sciences, Stanford University, Stanford, California 94305, USA
**Department of Geosciences, University of Arizona, 1040 E 4th Street, Tucson, Arizona, 85721, USA
***U. S. Geological Survey, Menlo Park, 345 Middlefield Road, California 94025, USA
[†]Corresponding author: Present address: U. S. Geological Survey, 345 Middlefield Road, MS 901, Menlo Park, California 94025, USA; jcolgan@usgs.gov
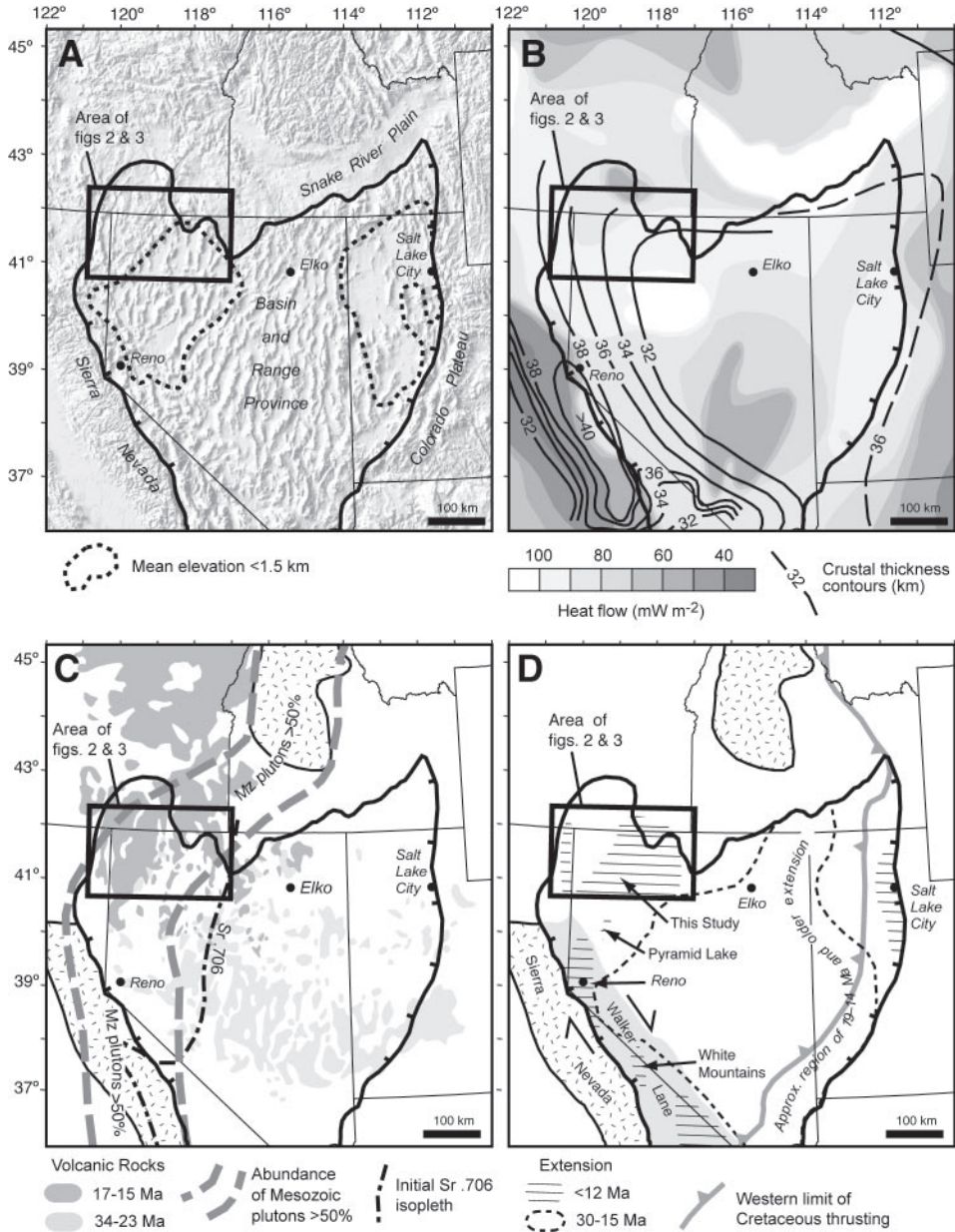
Fig. 1. Maps of western United States, showing location of study area (black square) in Basin and Range Province (heavy black outline with barbs). (A) Shaded-relief map showing major physiographic features discussed in the text; areas of low elevation within the Basin and Range shown by dashed outlines. (B) Heat flow (Blackwell and others, 1991) and approximate crustal thickness (Mooney and Weaver, 1989) in California and western Nevada; modified with data from Fliedner and others (2000) in the southern Sierra. (C) Distribution of Cenozoic volcanic rocks (Christiansen and Yeats, 1992) and approximate extent of Cretaceous batholith (zone of >50% Mesozoic plutons from Barton and Hanson, 1989). (D) Areas of 19–14 Ma and older extension (Dilles and Gans, 1995), western limit of Cretaceous thrusting (DeCelles and Coogan, 2006), and regions of ≤12 Ma extension (this study; Henry and Perkins, 2001; Stockli and others, 2003; Whitehill and others, 2004).

(Miller and others, 1999; Stockli and others, 2001; Surpless and others, 2002; Stockli, 2005). In many areas, these faults cut and expose older extensional structures that formed during Eocene-early Miocene time (for example; Smith, 1992; Miller and others, 1999; Hudson and others, 2000; Egger and others, 2003; Howard, 2003) and the magnitude of Cenozoic extension across the province is >50 percent (for example; Smith and others, 1991). Today, central Nevada is characterized by 31 to 36 km thick crust (fig. 1B; Klemperer and others, 1987), high mean elevations (>1.8 km), and moderately elevated heat flow ($\sim$50 – 80 mW m^{-2}; fig. 1B; Blackwell and Steele, 1992). Volcanism in this region peaked in the late Oligocene - early Miocene (34 – 23 Ma) with the eruption of voluminous calc-alkaline ash-flow tuffs (fig. 1C) and was coeval with early extension. Subsequent eruptions have been minor in volume (for example; Christiansen and Yeats, 1992) and the main phase of Miocene extension (19 – 14 Ma) was largely amagmatic.

Studies of individual ranges in northwestern Nevada (Colgan and others, 2004, 2006) indicate that extensional faulting began more recently and represents substantially less total strain than does extensional faulting in central Nevada. Today, northwestern Nevada is underlain by similar $\sim$31 km thick crust (Lerch and others, 2005a; fig. 1B), but is characterized by lower mean elevations (<1.5 km; fig. 1A) and higher heat flow (>100 mW/m^2; fig. 1B, for example; Blackwell and Steele, 1992). In contrast to central Nevada, where major volcanism had largely ceased by early Miocene time, northwestern Nevada was the site of voluminous middle Miocene bimodal volcanism (fig. 1C, for example; Christiansen and others, 1992) that is often attributed to the initial impingement of the Yellowstone hotspot at 16.5 Ma (for example; Pierce and Morgan, 1992). Thus, although northwestern Nevada today is physiographically similar to the Basin and Range Province at large, it appears to have undergone a significantly different history of both volcanism and extension.

The goal of this study is to establish the magnitude and timing of extension across the region shown in figures 2 and 3, and to use this information to evaluate the pre-extensional thermal and structural condition of the crust. First, we synthesize regional geologic and geochronologic data that establish the timing of volcanism and the magnitude of Cenozoic crustal extension. We then integrate this data set with new fission-track and (U-Th)/He thermochronologic data that constrain both the timing and rate of Cenozoic extensional faulting and the amount and timing of pre-extensional cooling and exhumation of the pre-Tertiary basement complex.

Cretaceous granitic basement rocks in northwestern Nevada were unroofed during the Late Cretaceous from depths of about 5 km. A subsequent period of relative tectonic quiescence persisted throughout Oligocene and Miocene volcanism and ended with the onset of Basin and Range extension at about 12 Ma. Compared to the central Nevada Basin and Range, extension in northwestern Nevada began more recently (12 Ma), is of lesser total magnitude ($\sim$12%), and was accommodated entirely by high-angle normal faults. The low magnitude of extension and early Tertiary stability suggest that the modern $\sim$31 km thick crust in northwestern Nevada was only slightly thicker ($\sim$35 km) prior to extension and was no thicker than $\sim$38 km in the Late Cretaceous. This stands in contrast to other parts of the Basin and Range, where the crust was thickened to at least 45 to 50 km by Cretaceous thrusting and subsequently thinned to $\sim$30 km by large magnitude (>50%) extension.

REGIONAL GEOLOGIC SETTING

Pre-Tertiary Geology

Paleozoic and Mesozoic basement rocks crop out extensively in the eastern part of the study area but are largely covered by Cenozoic deposits to the west (fig. 3). To the
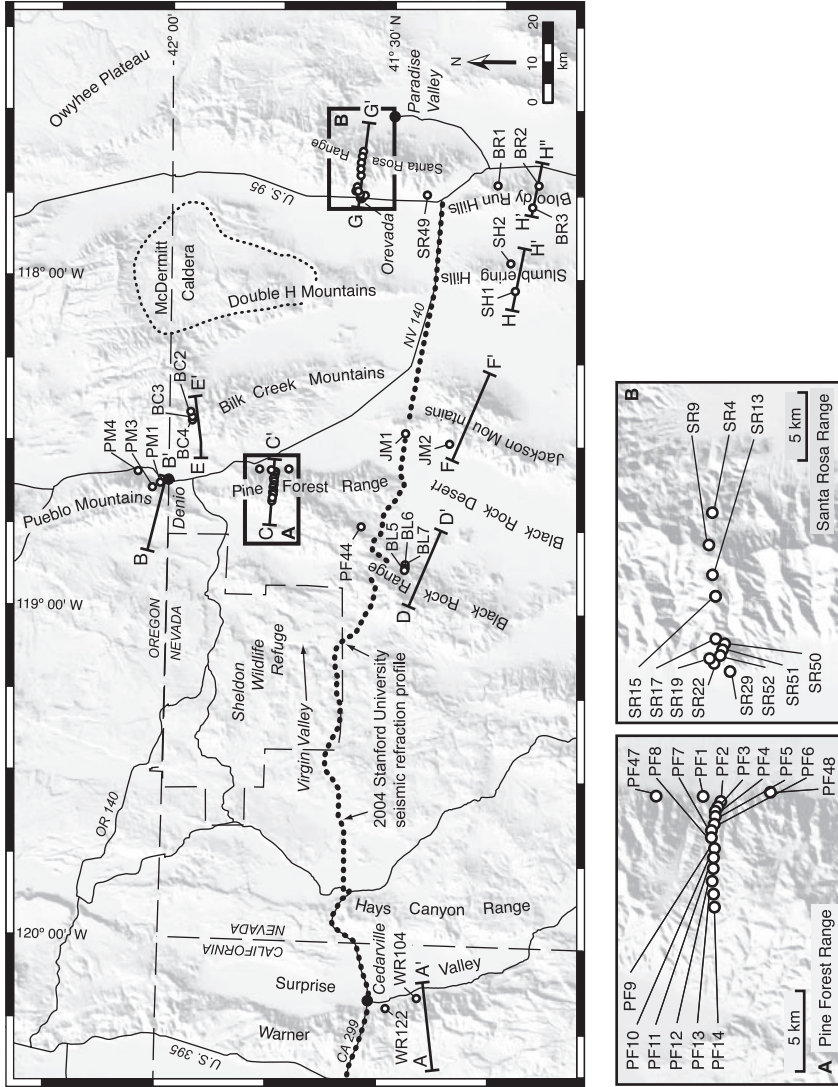
Fig. 2. Shaded-relief map of study area, showing sample locations and numbers, features discussed in the text, and location of cross sections in figure 4. Base map from USGS National Elevation Dataset (*http://ned.usgs.gov*).
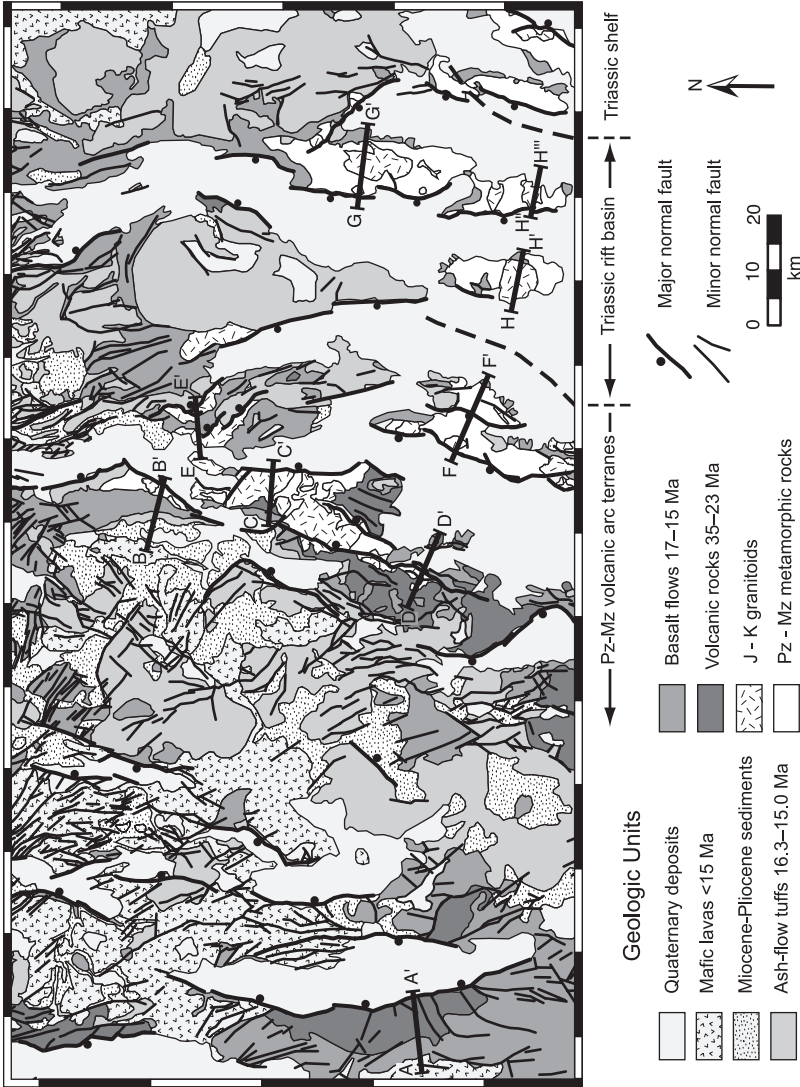
Fig. 3. Simplified geologic map of study area (same scale and extent as fig. 2), showing geologic units discussed in the text and location of cross-sections in figure 4. Geology modified from state geologic maps of Nevada (Stewart and Carlson, 1978), California (Jennings and others, 1977), and Oregon (Walker and MacLeod, 1991).

east, basement rocks consist of fine-grained Triassic siliciclasic rocks (fig. 3) deposited in deep marine rift-basins that developed across the Permo-Triassic Sonoma orogenic belt (Wyld, 2002; Wyld and others, 2003). To the west of these units, basement rocks consist of Paleozoic–early Mesozoic volcanic arc terranes (fig. 3; for example; Wyld and Wright, 2001). Both the Triassic basin deposits and adjacent arc rocks were deformed in the Early to Middle Jurassic during development of the Luning-Fencemaker fold-thrust belt (Wyld and others, 2003). Arc strata were deformed under greenschist to amphibolite-facies conditions and thrust eastward over the Triassic rift-basin deposits, which were isoclinally folded and metamorphosed to greenschist facies (Wyld, 2002; Wyld and others, 2003).

The Paleozoic and early Mesozoic rocks are intruded by Mesozoic, predominantly Cretaceous (98 – 116 Ma; this study; Wyld and Wright, 2001), granitic plutons that make up over 50 percent of the exposed basement in the central part of the study area (fig. 3). These plutons are broadly similar in age and composition to plutons presently exposed in the Sierra Nevada and were likely once contiguous with the main Sierra Nevada batholith prior to disruption by extensional faulting (fig. 1C; for example; Smith and others, 1971; Wyld and Wright, 2001). It is important to note that, where mapped in detail, basement rocks in the modern fault blocks across northwestern Nevada are not cut by earlier sets of normal faults that predate the modern range-bounding faults (for example; Compton, 1960; Wyld, 1996; Quinn and others, 1997; Wolak, ms, 2001). They are cut and uplifted only by the same sets of high-angle normal faults that cut and tilt the overlying Cenozoic rocks and bound the modern ranges (fig. 3).

Cenozoic Rocks

Cenozoic rocks in northwestern Nevada are predominantly volcanic and can be divided into two distinct age groups: Oligocene to early Miocene (35 – 23 Ma) lava flows and ash-flow tuffs and middle Miocene (17 – 15 Ma) basalt-rhyolite sequences (fig. 3). Eocene (38 Ma) andesitic rocks crop out sparsely in the Pine Forest Range (Colgan and others, 2006), and younger late Miocene and Pliocene basalt flows locally overlie older rocks in the Sheldon Wildlife Refuge (fig. 2; Greene, 1984) and on the east side of Surprise Valley (fig. 2; Carmichael and others, 2006), but these rocks are volumetrically minor compared to the Oligocene and Miocene rocks.

Older (35 – 23 Ma) volcanic rocks crop out primarily in the western part of the study area, in the Pine Forest Range (Colgan and others, 2006), Black Rock Range (Lerch and others, 2005b), and Warner Range (Duffield and McKee, 1986). They are presumed to be present beneath younger Miocene rocks in the intervening California-Nevada border region. These rocks are bimodal and consist primarily of basalt-basaltic andesite lava flows interbedded with widespread dacitic-rhyolitic ignimbrites and lava flows (Colgan and others, 2006). Moderate topography (up to 300 m) existed at the time these rocks were deposited, but the regional distribution of units suggests no major topography (that is, no large mountain ranges). In the Warner Range (fig. 4A), Oligocene lava flows equivalent in age (25 – 26 Ma) to units in the Pine Forest and Black Rock Ranges (figs. 4C and 4D) overlie a thick sequence (>1.5 km, fig. 4A) of 34 Ma and older volcanoclastic and conglomeratic sedimentary rocks (Duffield and McKee, 1986). These conglomerates crop out nowhere else in the study area. The overlying Oligocene units thin to the east and crop out in the Pine Forest and Black Rock Ranges but are largely absent east of the Jackson Range and Bilk Creek Mountains (fig. 3).

Middle Miocene (ca. 17 – 15 Ma) basalts and overlying rhyolitic ash-flow tuffs crop out extensively across northwestern Nevada and have been interpreted as the earliest eruptions of the Yellowstone hotspot (for example; Pierce and Morgan, 1992). Basalt
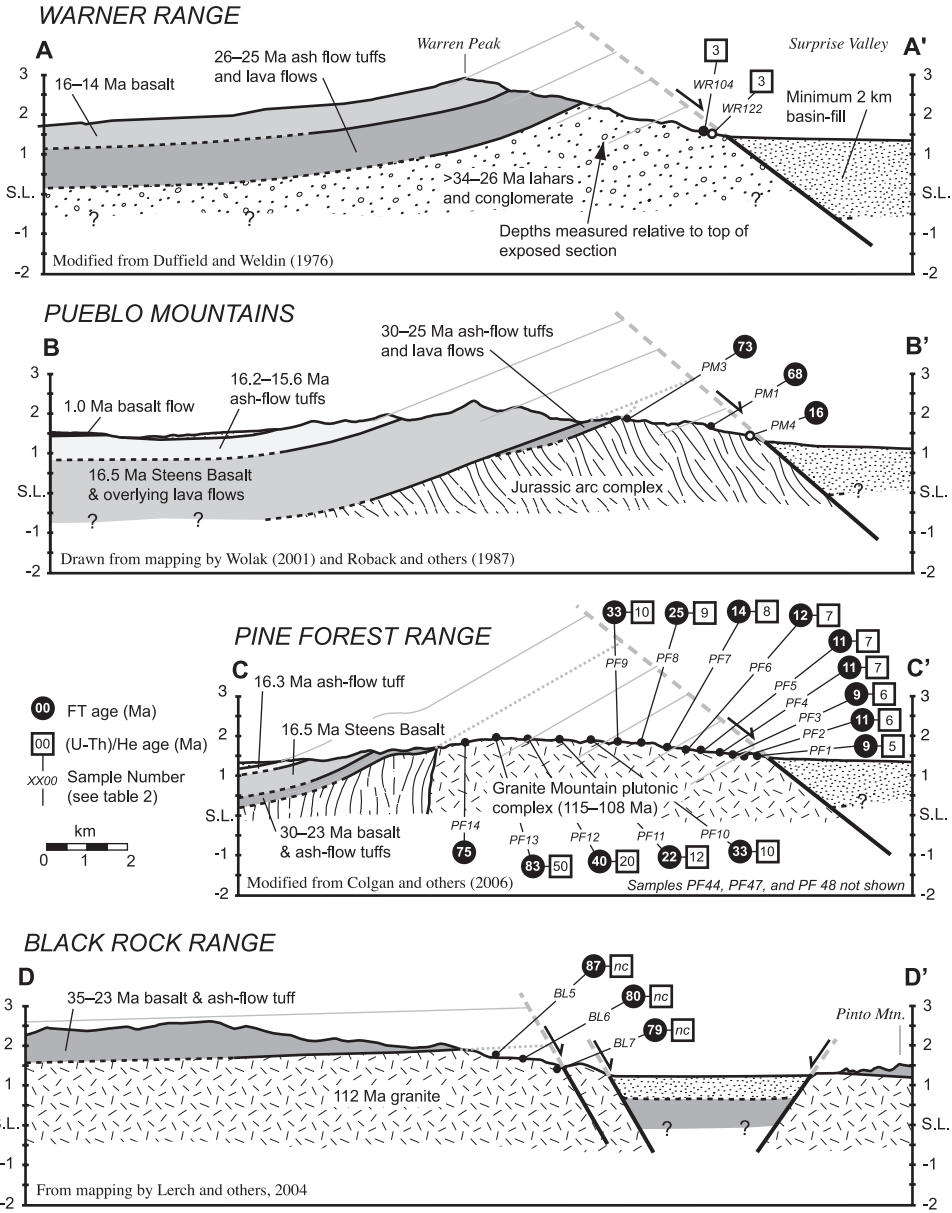
Fig. 4. Geologic cross-sections of ranges discussed in the text, showing structural positions of samples (small black circles) analyzed in this study. Open circles indicate samples projected into the line of section from >1 km away. All ages (table 1) are rounded to the nearest Ma. (U-Th)/He ages are the mean of two single grain ages, represented by "nc" where the two ages differ by >20%. Sources of data shown on individual cross sections. Elevations are km above and below sea level (S.L.); thin gray lines are paleodepths (km) above and below the basal Tertiary unconformity (dashed line).

flows are thickest to the north in the Pueblo Mountains (>1 km) and thin to the south, cropping out in the Pine Forest Range and Bilk Creek Mountains but largely absent in the Black Rock Range and to the east of the Jackson Range (figs. 2 and 3). Where mapped in detail, middle Miocene rocks conformably overlie older volcanic rocks
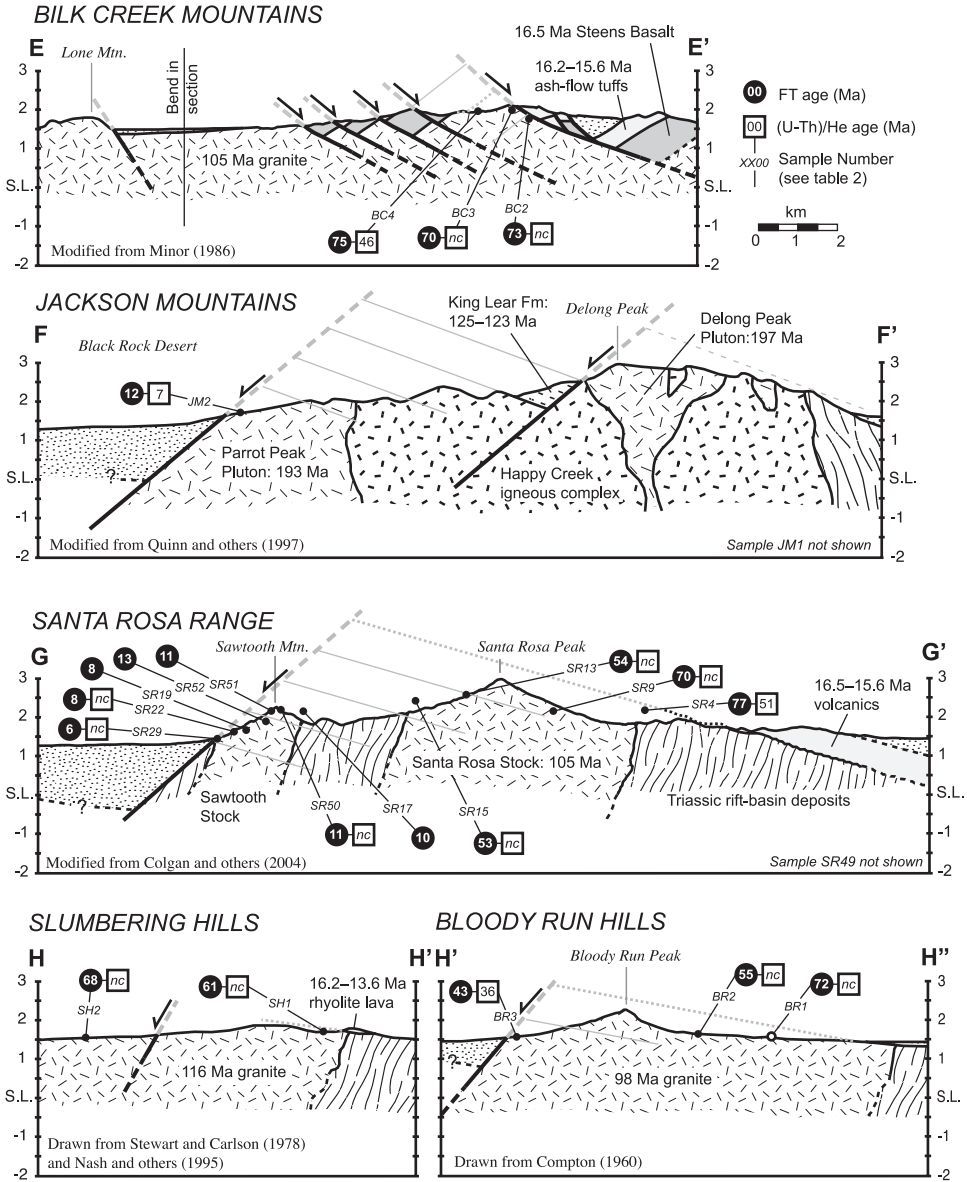
Fig. 4. (Continued)

(Lerch and others, 2005b; Colgan and others, 2006), indicating no significant tilting and extensional faulting between 35 and 15 Ma. Miocene (16.3 – 15.0 Ma) ash-flow tuffs (Noble and others, 1970; Rytuba and McKee, 1984) are cut and tilted by the major normal faults throughout the region shown in figures 2 and 3, providing a maximum age (15 Ma) for the onset of Basin and Range extension. In the northern Slumbering Hills and northernmost Jackson Range, younger rhyolite lava flows (13.6 and 14.6 Ma, respectively) are cut by range-bounding faults, providing local evidence for faulting younger than ~14 Ma (Nash and others, 1995; Castor and Henry, 2000).

The apatite fission-track and apatite (U-Th)/He systems have been used to date the timing of slip on major normal fault systems in many parts of the Basin and Range Province (for example; Fitzgerald and others, 1991; Foster and others, 1993; Miller and others, 1999; Armstrong and others, 2003; Stockli, 2005), and, under favorable conditions, can also constrain the actual rates of cooling, exhumation, and fault slip (for example; Ehlers and others, 2003). In this study, fission-track and (U-Th)/He ages document the timing and rate of Cenozoic extensional faulting in northwestern Nevada as well as the pre-extensional, Late Cretaceous - early Tertiary cooling history of the region.

Fission-track analysis is based on the spontaneous fission decay of ^{238}U, which expels high-energy nuclear fragments that create linear damage trails in the host crystal (for example; Tagami and O'Sullivan, 2005). Fission-tracks form at a constant rate with an essentially constant initial length and are progressively annealed (erased) at elevated subsurface temperatures, causing measurable reductions in both track length and apparent sample age (for example; Gleadow and others, 1986; Green and others, 1989). In apatite, fission-track ages are totally reset to zero age at subsurface temperatures greater than ~110 to 135°C, generally equivalent to subsurface depths greater than ~3 to 5 km. Ages are partially reset over the temperature range ~60 to 120°C, termed the partial annealing zone (PAZ; for example; Green and others, 1989; Dumitru, 2000). Qualitatively, longer, tightly clustered track-length distributions indicate rapid cooling, while broadly distributed clusters of shorter lengths indicate slower and or/irregular cooling through the temperature interval ~60 to 120°C (for example; Gleadow and others, 1986; Green and others, 1989). The cooling history of a fission-track sample can be modeled more rigorously using computer programs that determine an array of possible time-temperature paths consistent with a given sample age and length distribution; modeled cooling paths for this study were generated using the FTSolve program of Ketcham and others (2000).

(U-Th)/He thermochronology is based on the production of ^{4}He by the alpha decay of U and Th (for example; Zeitler and others, 1987; Farley, 2002). In apatite, He is lost by volume diffusion at elevated temperatures, and the closure temperature of the apatite (U-Th)/He system is affected by several factors, including the cooling rate and size (radius) of the apatite grains (for example; Wolf and others, 1998; Farley, 2000). Diffusion experiments on natural apatite crystals indicate an average closure temperature of ~68 ± 5°C for average-sized (<50 – 150 μm radius) apatite grains, assuming a cooling rate of 10°C/km (Farley, 2000). For apatite held at relatively constant temperatures over geologic timescales (10 – 100 m.y.), Wolf and others (1998) define an apatite He partial retention zone (PRZ) as the temperature range (40 – 85°C) over which the measured age of a sample is reduced from 90 percent to 10 percent of the holding time. Based on geologic evidence and fission-track data from the same samples, it is reasonable to assume that our samples were held essentially isothermally for a long period (>40 m.y.) prior to relatively rapid exhumation along normal faults; we therefore use Wolf and others' (1998) definition of the PRZ and interpret it in a fashion analogous to the fission-track PAZ. When considering the age of an individual sample, we assume a closure temperature of 65°C, due to the smaller average size of our apatite grains (67 μm radius, table A1) compared to those of Farley (2000), who calculated $T_c = 68°C$ for 100 μm radius grains.

To date the time of slip on major normal faults, systematic transects of samples are collected across the footwall of the fault system in order to obtain samples that resided at the widest possible range of paleodepths, and thus paleotemperatures, before extension and exhumation began. Detailed explanations of this application are given in Foster and John (1999), Miller and others (1999), and Stockli (2005). Given

sufficient fault throw to exhume rocks that resided at high enough temperatures prior to faulting (>120°C for apatite fission track and >85°C for apatite (U-Th)/He), samples from deeper paleodepths in a tilted fault block (close to the range-bounding fault) record information about the timing and rate of exhumation and faulting, while samples from shallow (generally <1 – 2 km) paleodepths retain information about the pre-faulting thermal history. The pre-extensional paleodepth of the exhumed fission-track PAZ and (U-Th)/He PRZ can also be used to estimate the pre-extensional geothermal gradient (for example; Dumitru, 1990; Howard and Foster, 1996; Stockli and others, 2003).

THERMOCHRONOLOGIC DATA

Fission-track data have previously been reported from the Santa Rosa Range and the Pine Forest Range (Colgan and others, 2004, 2006). In this study, additional fission-track ages were obtained from surrounding ranges, and single-grain (U-Th)/He ages were obtained from both new samples (this study), and from previously analyzed fission-track samples (table 1). Fission-track and (U-Th)/He ages are presented on a range-by-range basis (fig. 4). For each range we briefly summarize relevant geologic relationships that bracket the timing and amount of extension (table 2), present the thermochronologic data (table 1), and summarize the timing of both pre-extensional cooling and subsequent extensional faulting. A description of analytical procedures and complete fission-track and (U-Th)/He analytical data is given in Appendices A and B (table B1, fig. B1, and table A1).

In the following sections we estimate the pre-extensional paleodepths (in km) of samples beneath two different paleohorizontal reference datums. We use "D_s" to denote the paleodepth of a sample beneath the land surface prior to the onset of extension, which is useful when interpreting fission-track and (U-Th)/He ages that document the timing of extension and the geothermal gradient prior to faulting (figs. 5, 6, and 7). We use "D_u" to denote the paleodepth of a sample beneath the basal Tertiary unconformity by subtracting the thickness of overlying Tertiary volcanic rocks from D_s. This provides an approximation of depth beneath the early Oligocene land surface and is useful when interpreting cooling ages related to erosional unroofing of the pre-Tertiary basement (fig. 8).

Pine Forest Range (C–C')

The Pine Forest Range (fig. 4C) is underlain by Paleozoic-Mesozoic arc rocks deformed and metamorphosed in the early Jurassic and intruded by widespread Cretaceous (108 – 115 Ma) plutons that make up nearly 100 percent of the basement in the northern part of the range (Wyld and Wright, 2001). Overlying Cenozoic bimodal volcanic rocks form a conformable sequence that ranges in age from 30 to 16 Ma, is west-tilted up to 30°, and is bound on the east by an east-dipping (~40°) dip-slip normal fault (fig. 4C; Colgan and others, 2006). Regional gravity data (Saltus and Jachens, 1995) suggest that sedimentary fill in the adjacent valley is about 0.5 to 1 km thick on average, although these data are too coarse to resolve locally thicker portions of the basin. We assume ~1 to 2 km of sedimentary fill in the deepest part of the basin adjacent to the range-front fault, indicating a minimum of ~7 to 9 km of slip on the range-front fault and ~5 to 6.5 km of horizontal extension based on offset of the basal Tertiary unconformity (fig. 4C).

Seventeen samples were analyzed from the Pine Forest Range (table 1); fourteen from an E-W transect across the Cretaceous plutonic complex in the northern part of the range, two from the range-front north (PF47) and south (PF48) of the main transect, and one from the southwestern part of range (PF44). In general, these samples yielded abundant, high-quality apatite, with the exception of sample PF47, which yielded low-quality apatite characterized by numerous dislocations and inclu-

TABLE 1

Thermochronology sample locality and age data

Sample Number	Latitude (°N)	Longitude (°W)	D_u (m)[†]	D_s (m)[‡]	FT Age (Ma ± 1σ)[§]	Mean Track L. (µm ± 1σ)[#]	He Age (a) (Ma ± 1σ)	He Age (b) (Ma ± 1σ)
Warner Range (A–A')								
JC04-WR122	41° 28' 27"	120° 11' 11"		3800			3.0 ± 0.4	2.0 ± 0.1
JC04-WR104	41° 24' 10"	120° 09' 24"		3800			3.3 ± 0.1	3.2 ± 0.1
Pueblo Mountains (B–B')								
JC02-PM1	41° 58' 30"	118° 40' 15"	1220	3220	67.9 ± 3.1	13.45 ± 0.08 m		
JC02-PM3	42° 01' 54"	118° 39' 53"	100	2100	73.2 ± 16.3	*no lengths*		
JC02-PM4	42° 00' 44"	118° 38' 35"	1585	3585	15.8 ± 1.8	12.71 ± 0.47 m		
Pine Forest Range (C–C'); FT ages from Colgan and others (2006)								
JC00-PF1	41° 46' 10"	118° 35' 27"	3810	4910	8.8 ± 1.1	13.85 ± 0.45 m	4.8 ± 0.1	5.6 ± 0.2
JC01-PF2	41° 45' 36"	118° 35' 41"	3780	4880	11.0 ± 1.0	13.31 ± 0.28 m	5.2 ± 0.2	6.3 ± 0.2
JC01-PF3	41° 45' 42"	118° 35' 54"	3630	4730	9.3 ± 1.0	13.83 ± 0.37 m	5.2 ± 0.2	6.3 ± 0.2
JC01-PF4	41° 45' 45"	118° 36' 06"	3440	4540	10.8 ± 1.0	14.05 ± 0.51	6.6 ± 0.2	6.8 ± 0.2
JC01-PF5	41° 45' 47"	118° 36' 21"	3240	4340	11.1 ± 1.0	14.03 ± 0.21 m	7.6 ± 0.2	6.4 ± 0.2
JC01-PF6	41° 45' 49"	118° 36' 41"	2960	4060	12.0 ± 1.0	13.76 ± 0.38	6.6 ± 0.2	7.4 ± 0.2
JC01-PF7	41° 45' 55"	118° 36' 58"	2740	3840	14.0 ± 1.2	13.08 ± 0.22 m	7.4 ± 0.2	7.7 ± 0.2
JC01-PF8	41° 45' 55"	118° 37' 17"	2470	3570	24.7 ± 1.9	12.10 ± 0.31 m	8.3 ± 0.2	8.9 ± 0.3
JC01-PF9	41° 45' 49"	118° 37' 46"	2010	3110	33.7 ± 1.8	12.57 ± 0.14 m	9.9 ± 0.3	10.4 ± 0.3
JC01-PF10	41° 45' 51"	118° 38' 11"	1710	2810	33.1 ± 1.7	12.67 ± 0.11 m	10.1 ± 0.3	9.2 ± 0.3
JC01-PF11	41° 45' 51"	118° 38' 40"	1320	2420	21.8 ± 1.1	14.67 ± 0.12 m	12.2 ± 0.4	12.6 ± 0.4
JC01-PF12	41° 45' 53"	118° 39' 14"	940	2040	39.2 ± 1.9	13.43 ± 0.10 m	19.9 ± 0.6	19.8 ± 0.6
JC01-PF13	41° 45' 51"	118° 39' 48"	520	1620	83.1 ± 2.8	13.61 ± 0.09 m	51.8 ± 1.6	46.9 ± 1.4
JC01-PF14	41° 45' 49"	118° 40' 23"	230	1330	75.0 ± 2.4	13.52 ± 0.09 m		
JC02-PF44	41° 34' 00"	118° 45' 20"	400	1500	79.3 ± 4.0	12.93 ± 0.09 m		
JC02-PF47	41° 47' 47"	118° 35' 28"	4110	5210	7.3 ± 1.0	*no lengths*	3.8 ± 0.2	5.4 ± 0.2
JC02-PF48	41° 43' 47"	118° 35' 12"	4270	5370	7.0 ± 0.7	14.06 ± 0.14 m	3.6 ± 0.1	3 ± 0.1
Black Rock Range (D–D')								
JC03-BL5	41° 28' 00"	118° 52' 32"	350	1350	87.0 ± 3.2	13.89 ± 0.07 m	64.6 ± 1.9	47.8 ± 1.4
JC03-BL6	41° 27' 54"	118° 52' 16"	650	1650	80.2 ± 3.7	13.85 ± 0.07 m	48.9 ± 1.5	608 ± 18.2
JC03-BL7	41° 27' 46"	118° 52' 06"	900	1900	78.7 ± 3.2	14.06 ± 0.07 m	58.5 ± 1.8	27.0 ± 0.8
Bilk Creek Mountains (E–E')								
JC02-BC2	41° 57' 18"	118° 25' 04"	1100	2600	73.3 ± 4.3	13.64 ± 0.11 m	154.4 ± 4.7	49.9 ± 1.5
JC02-BC3	41° 56' 53"	118° 25' 17"	750	2250	70.5 ± 5.2	12.84 ± 0.11 m	47.8 ± 1.4	40.1 ± 1.2
JC02-BC4	41° 56' 54"	118° 25' 36"	20	1520	75.3 ± 4.1	13.46 ± 0.13 m	47.6 ± 1.4	44.1 ± 1.3
Jackson Mountains (F–F')								
JC02-JM1	41° 29' 07"	118° 28' 05"	1500		82.3 ± 4.3	14.01 ± 0.11 m		
JC02-JM2	41° 21' 45"	118° 30' 53"	4100		11.7 ± 1.5	14.15 ± 0.15 m	6.7 ± 0.2	6.6 ± 0.2
Santa Rosa Range (G–G'); FT ages from Colgan and others (2004)								
JC00-SR4	41° 34' 50"	117° 37' 30"	150	950	77.1 ± 3.3	13.89 ± 0.12 m	50.8 ± 1.5	50.9 ± 1.5
JC00-SR9	41° 34' 58"	117° 39' 13"	790	1590	70.3 ± 4.5	13.30 ± 0.13 m	33.2 ± 1.0	41.6 ± 1.2
JC00-SR13	41° 34' 48"	117° 40' 48"	1040	1840	54.0 ± 3.0	13.82 ± 0.14 m	16.3 ± 0.5	26.3 ± 0.8
JC00-SR15	41° 34' 50"	117° 41' 44"	1570	2370	52.8 ± 2.5	13.38 ± 0.12 m	17.4 ± 0.5	21.4 ± 0.6
JC00-SR17	41° 34' 48"	117° 43' 53"	2560	3360	9.6 ± 0.8	14.28 ± 0.41		
JC00-SR19	41° 35' 01"	117° 44' 55"	3480	4280	8.1 ± 0.9	12.00 ± 1.25		
JC00-SR22	41° 34' 55"	177° 45' 08"	3630	4430	8.2 ± 0.6	14.01 ± 0.12 m	8.8 ± 0.3	8.9 ± 0.3
JC00-SR29	41° 34' 08"	117° 45' 34"	3930	4730	6.4 ± 0.8	13.88 ± 0.25 m	11.7 ± 1.0	14.8 ± 1.9
JC02-SR49	41° 26' 08"	117° 45' 31"	2300	3100	15.3 ± 1.6	13.10 ± 0.29 m	13.7 ± 0.6	40.9 ± 3.6
JC00-SR50	41° 34' 44"	117° 44' 01"	2620	3420	11.4 ± 0.9	13.85 ± 0.59 m	11.1 ± 0.3	13.9 ± 0.4
JC01-SR51	41° 34' 44"	117° 44' 17"	2740	3540	10.5 ± 0.8	13.25 ± 0.34 m		
JC01-SR52	41° 34' 56"	117° 44' 30"	3030	3830	13.2 ± 1.4	13.77 ± 0.31 m		
Slumbering Hills (H–H')								
JC02-SH1	41° 14' 46"	117° 58' 37"	200	800	60.7 ± 3.3	13.90 ± 0.10 m	63.7 ± 2.9	61.6 ± 2.5
JC02-SH2	41° 14' 25"	118° 01' 14"	900	1500	68.1 ± 4.4	13.77 ± 0.11 m	57.8 ± 5.1	81.3 ± 8.5
Bloody Run Hills (H'–H")								
JC02-BR1	41° 16' 07"	117° 44' 11"	300	1100	71.6 ± 4.2	13.62 ± 0.17 m	47.7 ± 3.3	57.3 ± 4.3
JC02-BR2	41° 10' 07"	117° 44' 30"	650	1450	55.0 ± 2.8	13.35 ± 0.12 m	36.6 ± 2.0	30.6 ± 1.8
JC02-BR3	41° 11' 03"	117° 47' 46"	1676	2476	43.0 ± 2.8	11.46 ± 0.20 m	36.5 ± 2.6	36.1 ± 2.5

[†]D_u denotes sample depth relative to the pre-faulting basal Tertiary unconformity.

[‡]D_s denotes sample depth relative to the pre-faulting land surface, including Tertiary volcanic and sedimentary overburden.

[§]FT Age is the fission-track central age of Galbraith and Laslett (1993).

[#]Mean Track L. is the mean fission track length for each sample, "m" indicates that length data was modeled. Only samples with >20 lengths were modeled. Model results are summarized in figures 9 and 10; all model results are presented in Colgan (2005).

<div align="center">

TABLE 2

Summary of geologic relationships

</div>

Locality (refer to figure 4)	Basement Age[†]	Tertiary Age[‡]	Tertiary thickness[§]	Approx. ~E–W extension[#]	Onset of faulting
Warner Range (A–A')	not exposed	>34–14 Ma	>3500 m	6 km	<14 Ma
Pueblo Mountains (B–B')	160–182 Ma	30–15 Ma	2000 m	5–6 km	<15 Ma
Pine Forest Range (C–C')	108–115 Ma	30–16 Ma	1100 m	4–5 km	11–12 Ma
Black Rock Range (D–D')	112 Ma	35–16 Ma	1000 m	1–2 km	<16 Ma
Bilk Creek Mountains (E–E')	105 Ma	21–15 Ma	2000 m	4–6 km	<15 Ma
Jackson Mountains (F–F')	193–197 Ma	16–14 Ma	not exposed	6–7 km	<14 Ma
Santa Rosa Range (G–G')	102–105 Ma	17–15 Ma	800 m	6–7 km	11–12 Ma
Slumbering Hills (H–H')	116 Ma	16–14 Ma	600 m	1 km	<14 Ma
Bloody Run Hills (H'–H")	98 Ma	17–15 Ma?	800 m	1.5 km	<15 Ma

[†]Crystallization age of basement plutons, used as the start time for fission-track length models.
[‡]Age range of exposed Tertiary volcanic and sedimentary rocks; all sections are conformable.
[§]Thickness of exposed Tertiary volcanic and sedimentary rocks, used to estimate sample paleodepths.
[#]Approximate magnitude of roughly E-W extension accommodated by slip on faults in the given range.
Sources of all data referenced in the text.

sions. Single-grain (U-Th)/He ages (two grains per sample) were obtained from thirteen of the samples in the main transect and two other range-front samples. This combined fission-track (Colgan and others, 2006) and (U-Th)/He (this study) data set
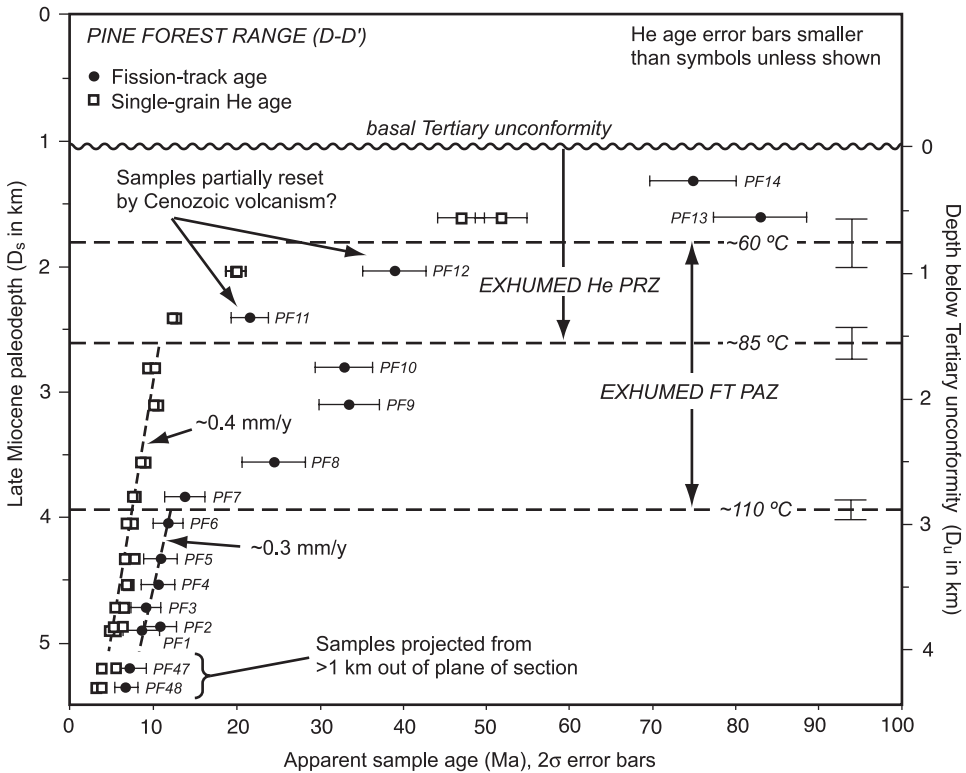

Fig. 5. Age vs. paleodepth plot for Pine Forest Range fission-track and (U-Th)/He samples. Fission-track data from Colgan and others (2006).
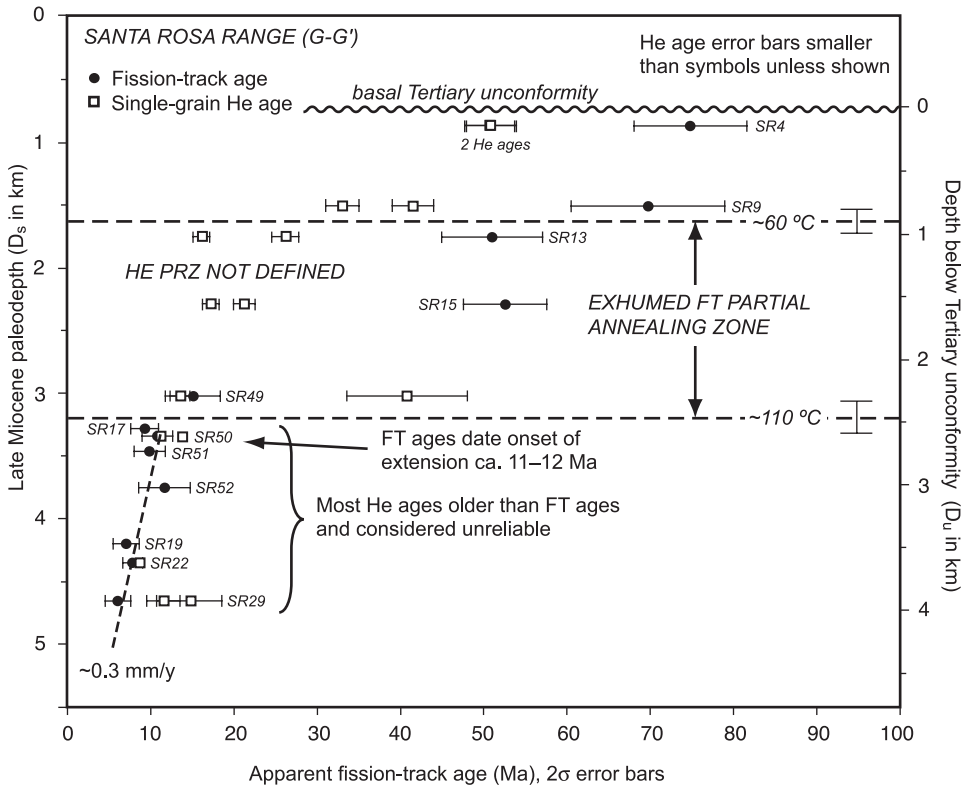
Fig. 6. Age vs. paleodepth plot for Santa Rosa Range fission-track and (U-Th)/He samples. Fission-track data from Colgan and others (2004).

provides the most detailed information about the timing and rate of extensional faulting in northwestern Nevada.

Samples from shallow paleodepths (D_s <2 km, fig. 5) were exhumed to near the surface prior to burial beneath 1 to 1.5 km of volcanic rocks over the interval 30 to 16 Ma (Colgan and others, 2006). These samples preserve Late Cretaceous (83 – 75 Ma) fission-track ages; modeled cooling histories indicate Late Cretaceous cooling (between 85 – 90 and 75 Ma), and are consistent with moderate reheating (~70°C) during Miocene burial, similar to the cooling history shown in figure 9A. (U-Th)/He data was obtained from one sample in this interval (PF13), which yielded an age of about 49 Ma (table 1; fig. 5). Single-grain He ages from shallow paleodepths analyzed in this study typically exhibit a wide range of ages (64 – 20 Ma; table 1, fig. 8), both between samples and between different grains from the same sample. These ages are interpreted to reflect partial resetting during burial beneath the overlying Tertiary volcanic section and are discussed in further detail in a later section. Fission-track ages from intermediate paleodepths ($D_s \approx$ 1.8–3.9 km) trend to overall younger ages, although several samples are younger (38 – 21 Ma) than would be expected in a simple intact exhumed fission-track PAZ (fig. 5). Modeled cooling histories for these samples are consistent with rapid cooling ca. 40 to 33 Ma. Several small 38 Ma intrusive bodies crop out nearby (within 1 km; Colgan and others, 2006), and we interpret cooling of these samples to represent local reheating during emplacement of these intrusive rocks or their deeper, unexposed equivalents, followed by varying degrees of partial resetting in the PAZ
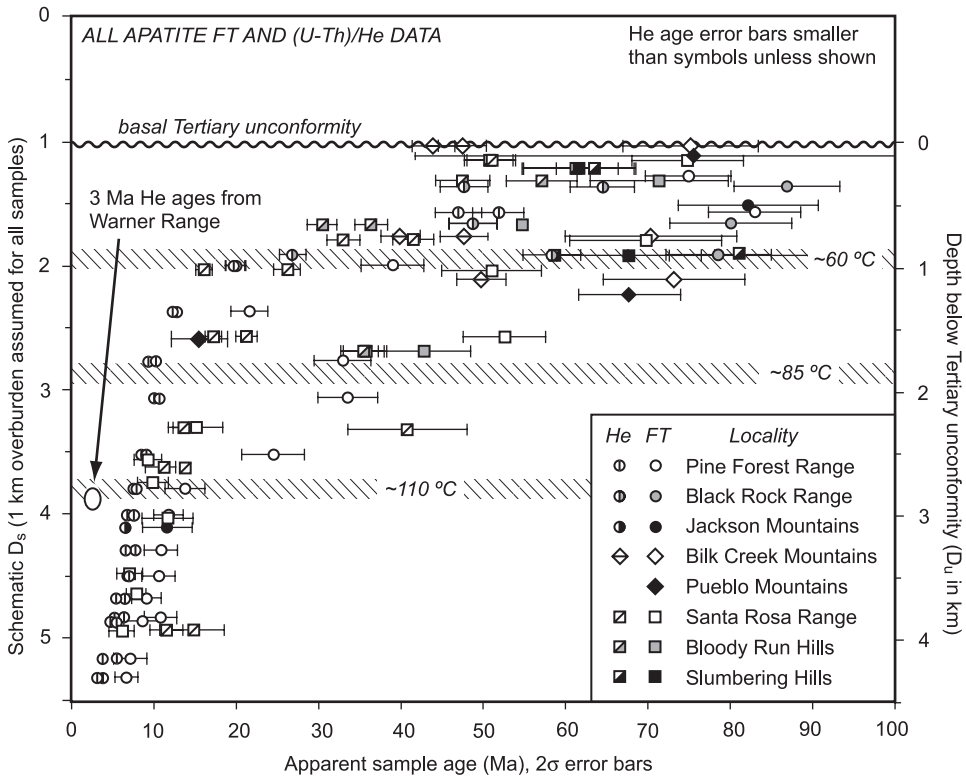
Fig. 7. Age vs. paleodepth (D_u) plot for all apatite fission-track and (U-Th)/He samples analyzed in this study. Isotherms are schematic assuming a 10°C surface temperature, 1 km of Tertiary overburden, and a 28°C/km geothermal gradient.

prior to exhumation. This interpretation is supported by undisturbed (U-Th)/He ages from this interval that trend uniformly younger and are characterized by reproducible single-grain ages within individual samples (fig. 5).

Fission-track ages from deeper paleodepths (D_s >3.8 km) decrease monotonically from 12 to 7 Ma (fig. 5) and are interpreted to record exhumation and uplift of the range during extensional faulting over this interval (Colgan and others, 2006). Modeled cooling histories from these samples show rapid late Miocene cooling (fig. 9D). The six deepest fission-track samples along the main transect (fig. 4) give an exhumation rate of ~800 m in 2.7 m.y. or ~0.3 km/m.y. (the two deepest samples are not included in this calculation since they are projected from out of the plane of the main transect, but they are consistent with a rate of 0.3 km/m.y.; fig. 5).

Single-grain (U-Th)/He ages from paleodepths of D_s >2.6 km decrease from 10 to 3 Ma and are interpreted to record exhumation and uplift of the range during extensional faulting over this interval (fig. 5). The onset of faulting is constrained by the break in slope in the He data between about 10 and 12 Ma ($D_s \approx 2.6$ km; fig. 5), consistent with our 12 Ma estimate for the onset of faulting based on the fission-track data. The ten (U-Th)/He ages from paleodepths of D_s >2.6 km along the main transect (10 − 5 Ma) give an exhumation rate of ~2.1 km in ~5 m.y. or ~0.4 km/m.y., compatible with the rate derived from the fission-track data (fig. 5).

Fission-track data from the Pine Forest Range define an exhumed fission-track PAZ with its base (110 ± 10°C) at D_s = 3.9 ± 0.1 km and its top (60 ± 5°C) at D_s =
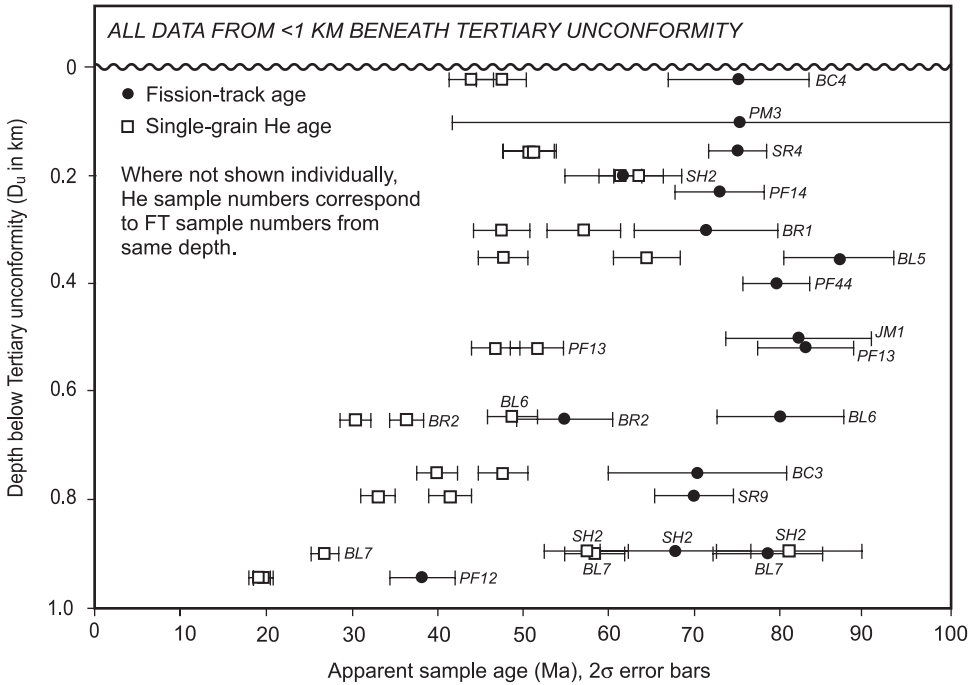
Fig. 8. Age vs. paleodepth (D_u) plot for all apatite fission-track and (U-Th)/He data less than 1 km beneath the Tertiary unconformity. Data are shown from the Santa Rosa Range, Bloody Run Hills, Slumbering Hills, Jackson Mountains, Bilk Creek Mountains, Black Rock Range, Pine Forest Range, and Pueblo Mountains.

1.8 ± 0.2 km (fig. 5). (U-Th)/He data define the base of an exhumed He PRZ (85 ± 5°C) at D_s = 2.6 ± 0.2 km paleodepth; the top of the PRZ is extrapolated to lie in the overlying Tertiary section. Assuming a surface temperature of 10 ± 5°C, these estimates yield a pre-extensional (ca. 12 Ma) geothermal gradient of 27 ± 5°C/km. This gradient is comparable to Miocene geothermal gradients estimated from other thermochronologic studies in the Basin and Range (for example; Fitzgerald and others, 1991; Foster and others, 1991).

Although apatite fission-track and (U-Th)/He dating are sensitive to relatively low temperatures, some exhumation must necessarily have taken place after the youngest samples cooled (in order to expose them at the surface). The youngest sample presently exposed in the Pine Forest Range (PF48) gives a (U-Th)/He age of 3 Ma. Assuming a nominal closure temperature of 65°C, a surface temperature of 10°C, and a stable geothermal gradient of 27°C/km, about 2 km of post-3 Ma exhumation is indicated by this sample.

The simplest interpretation of the Pine Forest Range data is that extensional faulting began about 11 to 12 Ma and continued at a moderate rate (about 0.3 – 0.5 km/m.y.) until close to the present time (<1 Ma). The exhumation rate indicated by the data is equivalent to fault-slip rates of 0.3 to 0.8 km/m.y. over the range of fault dips (70 – 40°) during the lifetime of the range-front fault. To first order, this slip rate is consistent with the estimated 8 km of slip on this fault in the past 12 m.y., but more detailed thermal modeling (for example; Ehlers and others, 2003) would be necessary to more rigorously constrain the relative rates of fault block uplift, fault slip, and horizontal extension. In any case, it is notable that the exhumation and fault slip rates
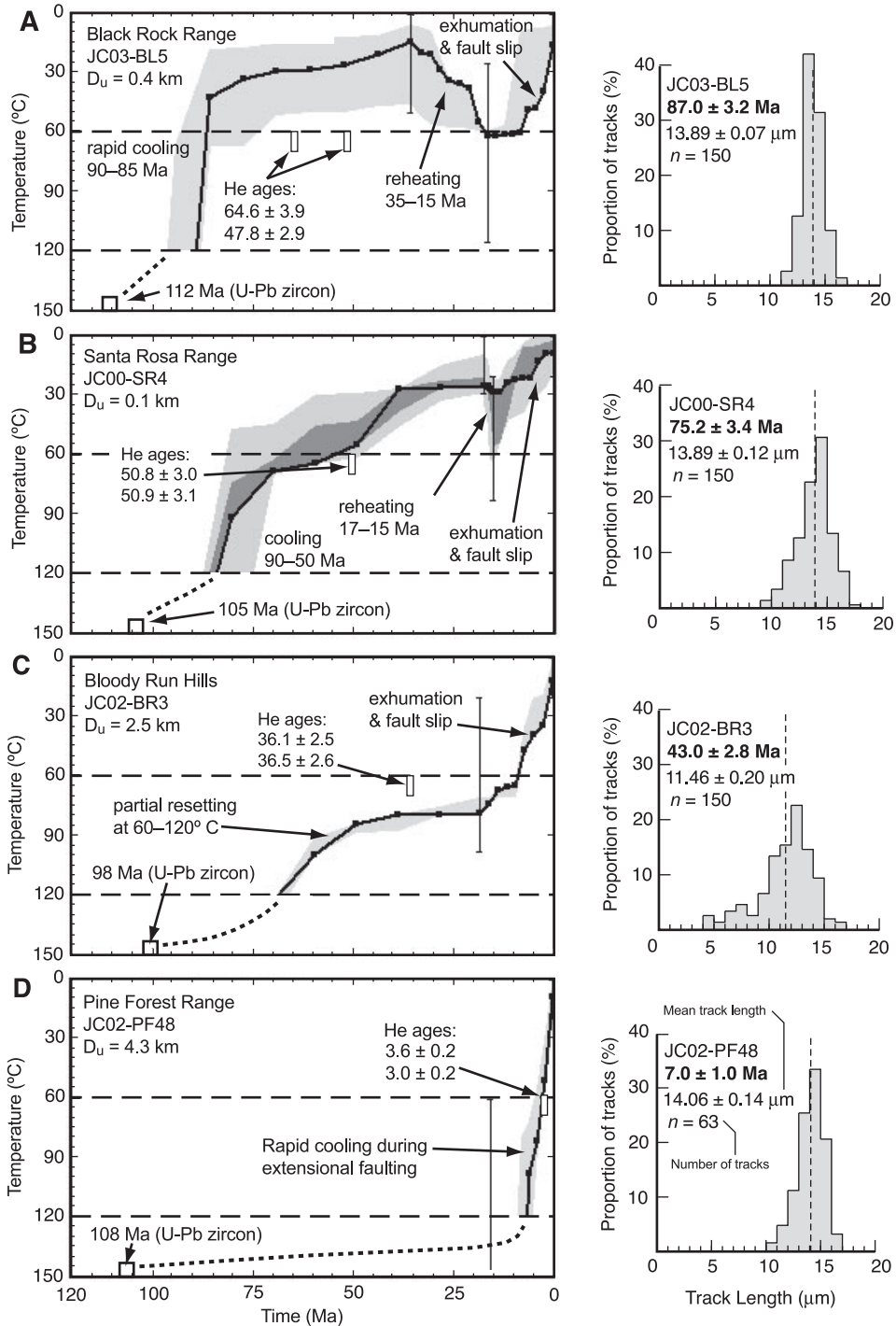
Fig. 9. Fission-track length data and cooling models for four representative samples analyzed in this study. Depths are given relative to the Tertiary unconformity (D_u). Cooling models: Heavy black line is preferred cooling path; dark gray shading is statistically good fit, light gray shading is statistically acceptable fit, thin black vertical lines are user-defined constraints on cooling envelope. Dashed horizontal lines denote temperature sensitivity window of models (120 – 60°C). Models generated with FTSolve (Ketcham and others, 2000). (U-Th)/He ages are shown for comparison to cooling paths and were not used to constrain models. A full description of fission-track analytical and modeling procedures is available in Appendix A, along with complete age and track length data.

derived from our data are distinctly slower and more protracted than rates derived from thermochronologic studies of many other Basin and Range fault blocks, where nearly depth-invariant apatite FT and U-Th/He ages record very rapid exhumation (up to 10 – 15 km over a few m.y.; for example; Fitzgerald and others, 1991; Howard and Foster, 1996; Miller and others, 1999; Reiners and others, 2000; Stockli and others, 2002; Carter and others, 2006).

Santa Rosa Range (G–G')

The Santa Rosa Range (fig. 4G) is composed of fine-grained Triassic rift-basin deposits metamorphosed to greenschist facies during the late Jurassic and intruded by extensive Cretaceous plutons (for example; Compton, 1960; Wyld and others, 2003). Basement rocks are unconformably overlain by ca. 17 to 15 Ma bimodal volcanic rocks (Breuseke and others, 2006) that are tilted ~15° east and bounded by a down-to-the-west, west-dipping (~40°), dip-slip fault (Colgan and others, 2004). About 8 km of slip on this fault accommodated about 6 km of E–W extension (fig. 4G).

Eleven samples of Cretaceous granite were collected along an E-W transect across the highest part of the range and one additional sample (SR49) from farther south along the range-front (figs. 2 and 4G). Samples from the 105 Ma Santa Rosa stock (U-Pb zircon; this study, Appendix C) in the core of the range (fig. 4G) yielded abundant, high-quality apatite, while samples from the undated Sawtooth stock close to the range-front fault (fig. 4G) yielded poor-quality apatite with abundant cracks, dislocations, and inclusions. Fission-track ages (table 1) from these samples were presented by Colgan and others (2004). In this study, new single-grain (U-Th)/He ages were obtained from 8 of these samples (2 grains per sample).

Shallow paleodepths (D_s <1.5 km) are characterized by Late Cretaceous (80 – 70 Ma) apparent fission-track ages (fig. 6); modeled cooling paths for these samples (fig. 9B) indicate Late Cretaceous (80 – 70 Ma) cooling. Slightly deeper ($D_s \approx 2.4$ km) samples have younger (54 – 52 Ma) apparent fission-track ages (fig. 6); modeled cooling paths for these samples show more protracted cooling from 120 to 60°C between 75 to 70 Ma and 45 Ma. The shallowest sample (SR4) yielded concordant single-grain He ages of 51 Ma, consistent with its modeled cooling time through 65°C from fission-track length data (fig. 9B). Single-grain He ages from deeper samples (1< D_s <2.4 km) range widely from 50 to 15 Ma (fig. 6) and grain ages within individual samples do not overlap within uncertainty. Fission-track data from the Santa Rosa Range define an exhumed fission-track PAZ with its base (110 ± 10°C) at 3.3 ± 0.2 km paleodepth and its top (60 ± 5°C) at 1.7 ± 0.2 km paleodepth. Assuming a surface temperature of 10 ± 5°C, these temperatures yield a pre-extensional geothermal gradient of 30 ± 6°C/km, similar to the 27 ± 5°C/km estimate from the Pine Forest Range.

At deeper paleodepths (D_s >2.5 km), fission-track ages decrease from 12 to 10 Ma to 6.4 Ma and are interpreted to date exhumation and uplift of the range during extensional faulting over this interval (fig. 6; Colgan and others, 2004). Assuming a stable geothermal gradient (~30°C/km), 1.3 km of exhumation from 11 to 6.4 Ma gives a rate of ~0.3 km/m.y. (fig. 6). Since 6.4 Ma, we estimate that an additional ~3 km of exhumation took place to bring the youngest sample (SR29) to the surface, equal to an exhumation rate of ~0.5 km/m.y. (assuming a surface temperature of ~10°C, a geothermal gradient of ~30°C/km, and a closure temperature of ~110°C). Uplift rates of 0.3 to 0.5 km/m.y. are similar to the apparent rates indicated by more detailed data from the Pine Forest Range. Unfortunately, single-grain (U-Th)/He ages from this interval (from the Sawtooth Stock, fig. 4G) scatter widely within individual samples and many are older than fission-track ages from the same sample (fig. 6). Although no obvious defects were observed in the analyzed grains, we attribute these

obviously spurious ages to unrecognized U-bearing inclusions, consistent with the generally poor quality of apatite grains observed in the fission-track grain mounts.

Based on the above data, we infer that extensional faulting in the Santa Rosa Range began ca. 12 to 11 Ma (slightly earlier than the previous 10 Ma estimate of Colgan and others, 2004) and was ongoing from 12 to 6 Ma. The amount of post 6 Ma exhumation is probably about 2 to 3 km (assuming a stable geothermal gradient), or at least half the total exhumation (~5 km) that took place along the range-front fault. The simplest interpretation of the data is that extension was ongoing in the Santa Rosa Range from ~12 Ma until close to the present time (probably <1 Ma) at a moderate rate of ~0.3 to 0.5 km/m.y., similar to the rate derived for the Pine Forest Range. Based on these exhumation rates, we infer similar fault-slip rates of 0.4 to 0.8 km/m.y., for the past 12 m.y. (along a fault dipping 55 – 40°), consistent with about 8 km total slip on the range-front fault.

Bloody Run Hills (H''–H''')

The Bloody Run Hills are composed of the same basement rocks as the Santa Rosa Range and are considered to be part of the same tectonic block (Compton, 1960). The southern of two granitic plutons in the range (fig. 3) yielded a U-Pb zircon age of 98 Ma (this study, Appendix C). The Bloody Run Hills are bounded to the west by a down-to-the-west normal fault; the dip and amount of slip on this fault are not known. Tertiary volcanic rocks crop out sparsely in the northern and southeastern parts of the range and are undated but assumed to be similar to 17 to 15 Ma rocks in the Santa Rosa Range (Compton, 1960). Assuming a moderate 10° east tilt of the range and ~0.5 to 1.0 km of basin fill, we estimate that 2.5 to 3 km of slip on the range-bounding fault accommodated at most ~2 km of E–W extension (fig. 4H).

Three samples were collected from the two Cretaceous plutons in the core of the range (fig. 3), two from shallow paleodepths (BR1 and BR2) on the east side and one (BR3) from deeper levels ($D_s \approx 1.4$ km, fig. 4H) adjacent to the range-front fault on the west side. Shallower samples gave apparent fission-track ages of 72 and 55 Ma (table 1); modeled cooling histories for these samples indicate cooling from 120°C to 60°C between about 75 to 60 Ma and 55 to 45 Ma (fig. 10). (U-Th)/He ages from these samples range from 31 to 57 Ma and do not overlap within uncertainty (table 1). The range-front sample (BR3) gave an apparent fission-track age of 43 Ma and a (U-Th)/He age of 36 Ma (mean of 2 grains; table 1). The modeled cooling history for this sample (fig. 9C) indicates long residence time (about 70 – 10 Ma) in the fission-track PAZ (120 – 60°C), and we interpret the fission-track and (U-Th)/He ages to have been partially reset during this interval. We infer that faulting in the Bloody Run Hills was coeval with faulting in the Santa Rosa Range, but was insufficient to exhume rocks with fully reset fission-track and (U-Th)/He ages.

Slumbering Hills (H–H')

The Slumbering Hills (fig. 4H) are underlain by Triassic rift-basin deposits intruded by a large Cretaceous granitic pluton (116 Ma; U-Pb zircon; this study, Appendix C). Overlying Tertiary volcanic rocks (16.2 – 13.6 Ma) exposed in the northwestern Slumbering Hills are up to 600 m thick and cut by down-to-the-west faults that expose paleodepths as deep as ~1 km (Nash and others, 1995). Despite the paucity of data on both surface geology and adjacent basin fill, we infer that the amount of E–W extension across the Slumbering Hills is small (probably 1 km or less), on the basis of low topography in the range, the absence of major mapped faults, and only moderate Tertiary dips (fig. 4H; Nash and others, 1995).

Two samples were collected from the granitic pluton in the central part of the range and yielded abundant, high-quality apatite (table 1). The shallower ($D_s \approx$ 200 m) eastern sample (SH1) yielded a fission-track age of 61 Ma and a (U-Th)/He age
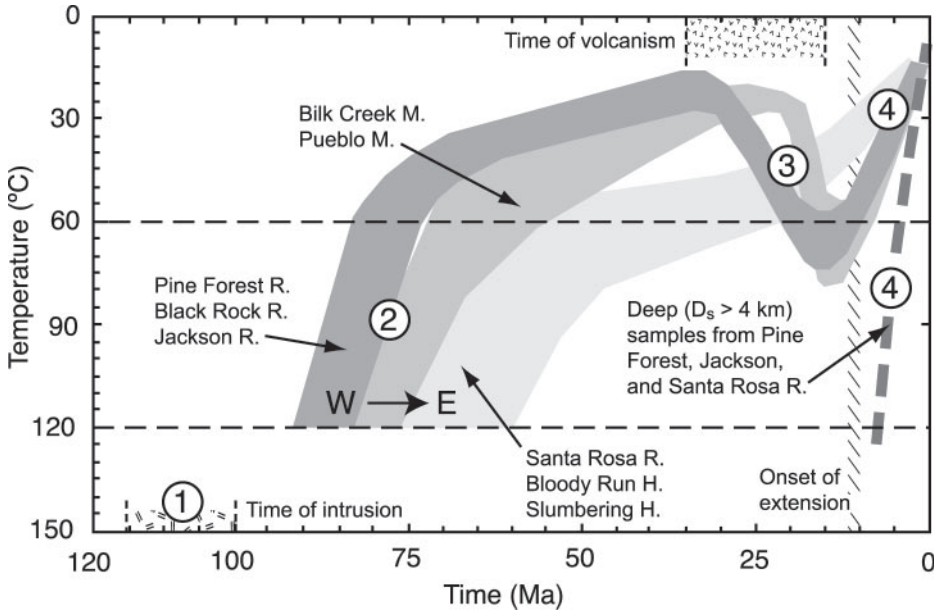
Fig. 10. Summary of cooling paths for all fission-track samples modeled in this study (*n* = 39). Gray shading encloses an envelope of the preferred cooling paths for the noted samples. Heavy dashed line denotes cooling paths of samples from deep structural levels. Numbers indicate: 1) Intrusion of plutons, 2) Late Cretaceous cooling, 3) Cenozoic burial and reheating ca. 35–15 Ma, 4) Late Miocene unroofing during extensional faulting.

of 63 Ma. The deeper ($D_s \approx 1$ km) sample (SH2) yielded an age of 68 Ma and (U-Th)/He ages of 57 and 81 Ma. Modeled cooling histories for these samples show 120 to 60°C cooling between about 70 and 60 Ma (fig. 10). We infer that extensional faulting took place more recently than 13.6 Ma but was not sufficient to exhume rocks from paleodepths greater than about 1 km.

Bilk Creek Mountains (E–E')

The northern Bilk Creek Mountains are underlain predominantly by Cretaceous granite (105 Ma; U-Pb zircon; this study, Appendix C), although Paleozoic volcanic arc rocks crop out sparsely in the southern part of the range (Jones, 1990). Basement rocks are overlain by the 16.5 Ma Steens basalt (~1 km thick) and overlying 16.3 to 15.0 Ma rhyolitic ash-flow tuffs (up to 1 km thick) erupted from the nearby calderas of the McDermitt volcanic field (Rytuba and McKee, 1984; Minor, ms, 1986). Minor and others (1989) report outcrops of 21.3 ± 0.7 Ma (K-Ar, whole rock) andesitic lava flows up to 200 m thick locally present beneath the Steens Basalt in the eastern part of the range; these rocks give a minimum age for the Tertiary unconformity. The Bilk Creek Mountains were therefore buried beneath ~2 km of volcanic rocks prior to faulting and uplift. Tertiary rocks are tilted up to 35° and cut by normal faults that expose granitic basement; total extension on these faults is about 4 to 6 km in the northern part of the range (Minor, ms, 1986) and an unknown but lesser amount to the south. Although the magnitude of extension is locally high (up to ~50%), it was accommodated by closely-spaced faults that do not expose deep structural levels (fig. 4E; Minor, ms, 1986; Minor and others, 1989; Minor and Wager, 1989).

Three samples of granite were collected from shallow paleodepths in the northern part of the range (table 1). All samples yielded abundant, high-quality apatite.

Fission-track ages range from 75 to 71 Ma and single-grain He ages range from 50 to 40 Ma (table 1; one grain yielded an unreasonably old 154 Ma age that we attribute to an unrecognized U-rich inclusion). Modeled cooling histories for these samples (fig. 10) show cooling from 120 to 60°C between about 80 and 65 Ma, and are consistent with moderate Miocene reheating and burial prior to late Miocene cooling during extensional faulting (similar to fig. 9A). Faulting is constrained to be younger than 15 Ma by tilted Tertiary rocks but was not sufficient to exhume rocks with fully reset fission-track or (U-Th)/He ages.

Jackson Mountains (F–F')

The Jackson Mountains (fig. 4F) are underlain by a volcanic arc complex consisting of late Paleozoic - early Mesozoic marine rocks intruded by the Triassic Happy Creek volcanic complex; these rocks are in turn intruded by several Jurassic granitic plutons and locally overlain unconformably by Cretaceous (123 – 125 Ma) clastic sediments of the King Lear Formation (fig. 4F; Quinn and others, 1997). Tertiary volcanic rocks are poorly exposed in the main part of the Jackson Mountains and data on their ages and compositions are largely absent, but rhyolite lava flows in the northernmost part of the range were dated at 14.6 Ma by Castor and Henry (2000). The Jackson Mountains are bounded on the west by a major down-to-west normal fault; the dip of this fault is not known but assumed to be about 40° by analogy to the major faults in the Santa Rosa and Pine Forest Ranges (fig. 4). In the northern part of the range, the Cretaceous King Lear Formation (up to 1.2 km thick) is tilted 25 to 30° E about a N-S axis and is bounded to the west by a down-to-the-west normal fault (fig. 4F) that Quinn and others (1997) interpret as Cretaceous. Geologic relationships provide no lower age limit for this fault, however, and at least some east-tilting of the King Lear Formation must result from E–W Cenozoic extensional faulting. The simplest interpretation is that tilting of the King Lear Formation is related to the adjacent normal fault and is entirely Cenozoic in age, fully consistent with 25 to 30° Cenozoic tilting of the nearby Pine Forest Range and northern Bilk Creek Mountains. We therefore interpret this fault as a Cenozoic fault related to uplift of the modern Jackson Mountains. Information on basin depth and structure beneath the Black Rock Desert to the west of the range are largely absent, but assuming 1 to 2 km of basin fill and restoring the King Lear Formation to horizontal yields ~7 to 8 km of horizontal extension related to motion on the two major faults (~7 km of slip on main fault and ~3 km of slip on the Delong Peak fault; fig. 4F).

Two samples were collected from Jurassic granites in the northern Jackson Range (table 1). The first (JM1) was obtained from the Deer Creek Pluton (196 Ma, U-Pb zircon; Quinn and others, 1997) at shallow paleodepths beneath the basal Tertiary unconformity ($D_u \approx 500$ m) in the northernmost part of the range. A second sample (JM2) was collected from the Parrot Peak pluton (193 Ma, U-Pb zircon; Quinn and others, 1997) at deeper paleodepths along the north-central part of the range front (fig. 4F). Because Tertiary rocks are not exposed in the main part of the range (section F-F') we measure the minimum paleodepth of sample JM2 ($D_s = D_u \approx 4$ km) beneath the top of the exposed Cretaceous sedimentary section, using the basal Cretaceous unconformity as a reference pre-extensional horizontal surface (fig. 4D). Both samples yielded small, poor-quality apatite grains. Fission-track ages were obtained for both samples and two single-grain He ages were obtained from the Parrot Peak sample (JM2).

The Deer Creek sample (JM1) has an apparent fission-track age of ~82 Ma and the modeled cooling history (fig. 10) shows rapid 120 to 60°C cooling between 85 and 75 Ma (similar to fig. 9A). The deeper sample (JM2) gave an apparent fission-track age of 11.7 ± 1.5 Ma and a (U-Th)/He age of 7.6 ± 0.4 Ma (mean of 2 single-grains). The modeled cooling history for this sample (similar to fig. 9D) indicates rapid 120 to 60°C

cooling from 12 to 11 Ma to the present. Although the onset of faulting cannot be pinpointed precisely, we infer it began about 12 Ma, the same time it began in the adjacent Pine Forest Range. Faulting was then ongoing from 12 to 7.6 Ma, with a further ~2 km of post-7.6 Ma uplift necessary to exhume sample JM2 (assuming the same thermal conditions as the Pine Forest Range). The absence of (U-Th)/He ages younger than 7.6 Ma does not necessarily indicate that faulting ceased before it did in the Pine Forest Range, but only that subsequent fault-slip was not enough to exhume samples with younger ages. The age of sample JM2 is comparable to samples from similar paleodepths ($D_s \approx 4$ km) in the Pine Forest Range (samples PF5 and PF6, table 1, figs. 6 and 7). Because extension in the northern Jackson Range was partitioned onto two major faults (fig. 4F), the total amount of vertical exhumation on the range-front fault is less than it is in the northern Pine Forest Range, where extension was accommodated by a single fault with correspondingly greater exhumation.

Pueblo Mountains (B-B')

The Pueblo Mountains (fig. 4B) are composed of metamorphosed Jurassic volcanic arc strata intruded by Jurassic plutons (182 – 160 Ma; Wyld and Wright, 2001; Wolak, ms, 2001). Basement rocks are overlain by ~1 to 1.5 km of Steens Basalt and related mafic lava flows erupted ca. 16.5 Ma (Roback and others, 1987; Hart and others, 1989). Basalt flows are overlain by a sequence of 16.3 to 15.0 Ma ignimbrites erupted from calderas of the nearby McDermitt volcanic field (Rytuba and McKee, 1984; Roback and others, 1987). Tertiary rocks in the range are conformably tilted 20° to 25° W and bounded by a major east-dipping fault on the east side of the range (figs. 3 and 4B). The dip of this fault is not known but assumed to be about 40° by analogy to the major faults in the Santa Rosa and Pine Forest Ranges. No data are available for the depth of basin-fill beneath adjacent Pueblo Valley, but assuming 1 to 2 km of fill, at least 4 km of E-W horizontal extension is likely with 6 to 7 km of slip on the range-front fault (fig. 4B). Based on the size and structural similarity of the Pueblo Mountains to the Warner Range where adjacent basin-fill is known to be >2 km deep (fig. 4A), the true amount of E-W extension is probably closer to 6 km.

Three samples were collected from Jurassic plutons and metavolcanic rocks (table 1), one (PM3) from close to the Tertiary unconformity ($D_u \approx 0.1$ km) and two (PM1 and PM4) from deeper levels ($1.3 < D_u < 1.6$ km) on the eastern range-front (fig. 4A). These samples yielded abundant but small ($<50\mu$m radius), poor-quality apatite that were judged unsuitable for (U-Th)/He dating. Shallow samples (PM1 and PM3; table 1) gave apparent fission-track ages of ~73 to 68 Ma. The modeled cooling history for sample PM1 (fig. 10) indicates 120 to 60°C cooling between about 80 and 60 Ma. The deepest sample (PM4) has an apparent fission-track age of 15.8 ± 1.8 Ma and a broad distribution of track lengths indicating incomplete resetting prior to extensional faulting. Faulting therefore began more recently than 15 Ma (the age of the youngest tilted Tertiary rocks), but was not sufficient to exhume rocks with fully reset apatite fission-track ages.

Black Rock Range (D–D')

The northern Black Rock Range (fig. 4D) is underlain by Cretaceous granite (112 Ma; U-Pb zircon; this study, Appendix C). Overlying volcanic rocks along the line of section D-D' range in age from 35 to 23 Ma (Lerch and others, 2005a); these rocks are overlain conformably by 16 to 15 Ma ignimbrites to the north of cross-section D-D' (fig. 4D; Noble and others, 1970). The Black Rock Range is gently tilted (~5°) along a down-to-the-east fault that exposes shallow ($D_u < 1$ km) pre-extensional paleodepths on the east side of the range. Detailed information on the structure of the basin east of the range is absent, but assuming no more than 0.5 km of basin fill (Saltus and Jachens,

1995), 2.5 to 3 km of slip on this fault and adjacent splays (fig. 4D) accommodated at most ~1 to 2 km of E–W extension.

Three samples of granite were collected from the east side of the range close to the range-front fault. Fission-track ages from these samples range from 87 to 78 Ma. Single-grain He ages (table 1) do not overlap within uncertainty, ranging from 59 to 27 Ma (one grain yielded an age of 608 Ma that we attribute to an unrecognized U-rich inclusion). Modeled cooling histories for these samples (fig. 10) all show 120 to 60°C cooling at about 85 to 90 Ma, and are consistent with reheating to ~65°C from 34 to 15 Ma during burial beneath the overlying Oligocene and Miocne volcanic rocks (fig. 9A). Extensional faulting is thus constrained by geologic relationships to be <15 Ma, but was insufficient to exhume rocks with fully reset apatite fission-track or (U-Th)/He ages.

Warner Range (A–A')

The Warner Range (fig. 4A) is composed entirely of Tertiary volcanic rocks and volcanoclastic sediments. Over 1.5 km of lahars and conglomeratic sediments as old as 34 Ma are exposed at the base of the section; the total thickness of the sequence and the depth to basement is not known (Duffield and McKee, 1986). Sediments are overlain by up to 1 km of andesitic lava flows and ignimbrites erupted at 26 to 25 Ma, which are in turn covered by up to 1 km of 16 to 14 Ma basalt flows (Duffield and McKee, 1986). This entire section is conformably tilted 20 to 25°W and bounded by a major down-to-the-east fault (fig. 4A). Geothermal wells indicate at least 2 km of basin fill in Surprise Valley (Duffield and McKee, 1986). Restoring the tilted Tertiary section to horizontal and removing slip (~7 – 8 km) along the range-front fault indicates a minimum of ~6 km of E–W horizontal extension. Although no rocks younger than 14 Ma are directly cut by the main range-front fault, late Miocene - Pliocene (8 – 3 Ma) basalt flows are cut and tilted by normal faults on the east side of Surprise Valley (figs. 2 and 3; Carmichael and others, 2006) and there is evidence for Quaternary slip on the range-front fault (Hedel, 1984).

Four samples were processed from volcanic clasts and matrix in the Tertiary volcanoclastic rocks, but none yielded any apatite. Very rare granitic clasts occur in conglomeratic intervals of these sediments near the base of the exposed section, however, and high-quality apatite was obtained from two granite clasts (samples WR104 and WR122, table 1). We estimate a minimum paleodepth of $D_s \approx 3.8$ km for these samples based on the thickness of the overlying section (fig. 4A). The two samples yielded single grain (U-Th)/He ages (mean of 2 grains per sample) of 3.3 Ma (WR104) and 2.5 Ma (WR122). We interpret these samples to have been fully reset (>85°C) prior to faulting and to reflect extension and fault slip ongoing at 3 Ma. These data support geologic evidence for faulting and extension more recently than ~3 Ma, but available data only constrain the onset of faulting to be more recent than 14 Ma.

DISCUSSION AND CONCLUSIONS

Kinematics of Basin and Range Extension in Northwestern Nevada

To estimate the total magnitude of extension across the study area, we first assume that no significant pre-Miocene extensional structures are present beneath flat-lying middle Miocene and younger rocks in the region between the Pine Forest and Warner Ranges (figs. 2 and 3). We consider this to be a reasonable assumption because no major pre-Miocene faults or angular unconformities have been documented on the margins of this little-extended area. Second, we assume that no significant extension took place anywhere in the study area prior to deposition of the earliest (Oligocene) volcanic rocks. Two observations support this interpretation: 1) the intact pre-Tertiary

basement geology and the absence of gently-dipping normal faults in the modern ranges, and 2) the preservation of Cretaceous fission-track ages everywhere beneath the basal Tertiary unconformity, indicating no significant exhumation and cooling since that time. Given these assumptions, the largest remaining source of uncertainty in our reconstruction is the depth and structure of the modern sedimentary basins, which makes it difficult to precisely estimate fault offset.

Although numerous minor faults are present throughout the study area (fig. 3), extension was accommodated almost entirely by the small number of widely-spaced, large-offset, predominantly N-S trending faults that uplifted the modern ranges (figs. 3 and 4). Where available, slip-indicators on these faults show dip-slip motion (Colgan and others, 2004, 2006). Slip on these faults thus resulted in E-W extension and westward motion of the Modoc Plateau relative to northern Nevada. Therefore, summing our range-by-range estimates of horizontal fault offset (table 2) on the major faults provides a good estimate of the total magnitude of horizontal E-W extension across the study area. From the Bloody Run Hills to the Black Rock Range (sections H, F, D, fig. 4), total extension is ~9 to 13 km over 115 km or 9 to 13 percent. From the Santa Rosa Range to the Pine Forest Range (sections A and G, fig. 4), total extension is ~12 to 15 km over 105 km, or 13 to 17 percent (assuming no more than 1 – 2 km total extension in the gently tilted Double H and southern Bilk Creek Mountains, fig. 2). Assuming about 15 km (~13%) extension over the eastern ~115 km of the study area (figs. 2 and 3), adding 6 km extension in the Warner Range (fig. 4), and assuming no more than 2 km extension in the Hays Canyon Range and minor intervening faults (fig. 2), the total E-W extension across the ~220 km study area (figs. 2 and 3) is ~23 km or ~12 percent.

The magnitude of extension decreases gradually to the north into the high lava plains of southern Oregon, where the modern high angle faults have not slipped enough to expose pre-Cenozoic basement (for example; Surpless, 2006). To the southeast of our study area, Smith and others (1991) estimate ~50 percent extension across much of central Nevada (~lat. 40° N, fig. 3D). South of Reno (fig. 3D), extension locally exceeds 100 percent (for example; Dilles and Gans, 1995; Surpless and others, 2002), but the exact magnitude of extension between our study area and these more highly extended domains is not known. Further work is necessary to determine if the total amount of extension increases progressively to the south, or if northwestern Nevada represents a distinct domain of low extension separated from more highly extended areas by a structural accommodation zone.

Having established the magnitude of Cenozoic extension across northwestern Nevada, we now turn to 1) the timing of extension and its relationship to deformation in the wider Basin and Range Province, 2) the magnitude and potential causes of Late Cretaceous regional cooling documented by our fission-track data, and 3) implications of our structural and thermochronologic data for the pre-extensional crustal structure in northwestern Nevada.

Timing and Regional Extent of Basin and Range Extension

The onset of extensional faulting in the study area (figs. 2 and 3) is everywhere constrained to be younger than ~15 Ma (locally 14 Ma) by volcanic rocks cut and tilted by major normal faults. Detailed thermochronologic data from the Pine Forest and Santa Rosa Ranges indicate a consistent 11 to 12 Ma age for the onset of faulting, and data from one sample in the Jackson Mountains is consistent with faulting beginning about 12 Ma. No other faults east of the Pine Forest Range have exhumed rocks from sufficient depths to directly date the onset of faulting. The simplest interpretation of our data is that faulting in the region between the Santa Rosa - Bloody Run Hills and Pueblo - Black Rock Ranges (fig. 2) began everywhere at 11 to 12 Ma.

The duration of faulting in this area is more difficult to determine, but apatite fission-track data from the Santa Rosa and Pine Forest Ranges demonstrate that it continued until at least 6 to 7 Ma. About 2 to 3 km of vertical offset along the range-bounding faults is necessary to complete the exhumation of samples presently exposed at the surface. Based on the modest rates indicated by the thermochronologic data (~0.4 km/m.y.), 2 to 3 km of exhumation would take an additional 5 to 8 m.y. A prolonged episode of faulting is supported by (U-Th)/He ages from the Pine Forest Range, which progressively decrease in age down to ~3 Ma (fig. 5), requiring ~1.5 to 2 km of additional exhumation to bring the youngest sample (PF48) to the surface (assuming a geothermal gradient of ~27°C/km). Recent paleoseismic work in the Santa Rosa Range (Personius and Mahan, 2005) documented a very low (<0.1 mm/y) slip rate for the last ~150 ka, indicating that modern fault-slip rates in that range are slower than the Miocene-Pliocene rates indicated by our data. Although rates of extension and uplift may vary on such short timescales, our data are most simply interpreted to record extensional faulting beginning about 12 Ma and continuing up to the present day at a moderately slow rate, consistent with geodetic data that indicates about 2 to 5 mm/y of approximately east-west extension across northwestern Nevada (Hammond and Thatcher, 2005).

It is unclear at present how faulting in the Warner Range relates to extension in northwestern Nevada. Geologic relationships and (U-Th)/He data indicate that significant faulting has taken place there more recently than 3 Ma, but the onset of extension is only directly constrained to be more recent than 14 Ma. The Warner Range may have begun forming at 12 Ma, during the same episode of faulting that formed the modern ranges in northwestern Nevada, or it may represent westward migration of Basin and Range faulting into this region during the Pliocene (compare Surpless and others, 2002).

Recent studies of Cenozoic basins and structures in the Reno area (fig. 1D) indicate an approximately 12 Ma age for the inception of extensional faulting and basin filling in the Verdi-Boca Basin and nearby basins (Trexler and others, 2000). With some local variation, these basins and associated structures were active until about 3 Ma, with an increasing component of strike-slip deformation as the northern Walker Lane strike-slip zone (fig. 1D) developed in the region from about 9 Ma to the present (Cashman and Fontaine, 2000). To the south of Reno, late Miocene extension and more recent strike-slip faulting overprinted earlier (ca. 15 Ma) extensional faulting (for example; Surpless and others, 2002), but in the area between Reno and Pyramid Lake (fig. 1) late Miocene faulting apparently took place in intact crust that was previously part of the Sierra Nevada (Trexler and others, 2000; Henry and Perkins, 2001). Preliminary studies of the region east of Pyramid Lake (fig. 3) suggest extensional faulting ongoing at 12 to 7 Ma and more recently (Whitehill and others, 2004). Recent work also indicates a 12 Ma age for the onset of major extension in the White Mountains to the south (fig. 3), although fault slip and exhumation of this range was much more rapid than it was in northwestern Nevada (Stockli and others, 2003). Late Miocene – early Pliocene extension in northwestern Nevada (this study) thus appears to be contemporaneous with extensional faulting along much of the western boundary of the Basin and Range (at least as far south as Reno), representing significant westward migration of the Basin and Range into previously little-extended crust.

Basin and Range extension arises from the complex interaction of several factors, including crustal buoyancy, basal tractions, and stresses originating at plate boundaries (for example; Sonder and Jones, 1999; Flesch and others, 2000). Regardless of the forces driving extension, however, plate reconstructions suggest that upper-crustal strain in the Basin and Range must be compatible with the position of the Pacific-North American plate boundary since about 18 to 20 Ma (Atwater and Stock, 1998).

Plate reconstructions indicate that the rate of Pacific plate motion (~N60° W relative to stable North America) increased from ~33 to ~52 mm/y at about 12 Ma, although this change was gradual and probably took place over at least 1 m.y. (Atwater and Stock, 1998; Argus and Gordon, 2001). Assuming a continental margin striking ~N30° W at this time (following Atwater and Stock, 1998), this change imparted an additional ~9 mm/y of plate-boundary-normal divergence (an increase from 14 to 23 mm/y) to the Pacific-North American plate margin at about 12 Ma. If continental deformation after 18 to 20 Ma is paced by divergence along the plate margin, a 12-Ma increase in the westward motion of the stable Sierra Nevada must be compensated by correspondingly increased rates of extension across the Basin and Range. Based on the timing of extension in northwestern Nevada and nearby areas described above, the 12 Ma onset of extension in the northwestern Basin and Range may be a consequence of increased late Miocene plate divergence. Extensional faulting was ongoing in many parts of central and eastern Nevada prior to 12 Ma, and the subsequent increase in extension rates may have favored the onset of extension in previously unextended crust on the western margin of the province. As better data become available on the timing and rates of Miocene extension in the northern Basin and Range, it should be possible to examine the relative rates of plate divergence and extension more rigorously, as has been done across the Basin and Range in the area around Las Vegas (Wernicke and Snow, 1998).

Magnitude and Timing of Late Cretaceous Exhumation and Cooling

Magnitude of late Cretaceous exhumation.—Cretaceous plutons in northwestern Nevada are dated at 115 to 98 Ma by U-Pb zircon (Wyld and Wright, 2001; this study, Appendix C). From these data, we infer that Cretaceous arc magmatism in northwestern Nevada took place from about 115 to 100 Ma and had largely ceased by 100 Ma. This interval is shorter than the full period of Cretaceous arc magmatism in the Sierra Nevada and predates the most voluminous episode of Sierran magmatism (100 – 85 Ma; for example; Saleeby and others, 2003). Ducea (2001) has suggested that this magmatic "flareup" resulted from underthrusting and melting of crustal material during Sevier crustal shortening; if this is correct it may explain the lack of 100 to 85 Ma plutons in NW Nevada, where granites were intruded into accreted crust hundreds of kilometers to the west of both the craton and the active Sevier thrust belt (fig. 1C).

Contact aureoles of plutons in northwestern Nevada are generally andalusite-bearing (Compton, 1960; Wyld, 1996), indicating maximum emplacement depths of ~11 km at most (for example; Barton and Hanson, 1989). The absence of preserved caldera remnants or other shallow volcanic features suggests at least ~3 km of post-intrusion erosion. Therefore we infer that the uppermost exposures of Cretaceous plutons directly beneath the Tertiary unconformity represent emplacement depths of 3 to 7 km, and the most deeply exhumed portions of the modern footwall blocks represent somewhat deeper emplacement depths up to ~11 km. We thus estimate that about 5 km (± 2km) of material was eroded from northwestern Nevada between the end of arc magmatism (ca. 100 Ma) and the deposition of Tertiary rocks beginning as early as 35 Ma. Similar 4 to 8 km emplacement depths and corresponding amounts of erosion have been determined for much of the northern Sierra Nevada to the south (for example; Ague and Brimhall, 1988). Based on the similar compositions, ages and exposure levels/metamorphic assemblages of plutons, we follow previous workers (Smith and others, 1971; Barton and Hanson, 1989) and infer that northwestern Nevada and adjacent parts of the Basin and Range to the south were contiguous with the northern Sierra Nevada batholith proper during the Late Cretaceous (fig. 1C).

Fission-track data from shallow samples ($D_u < 1\,km$).—Apparent fission-track ages from the shallowest exposed levels of plutons ($D_u < 1$ km; fig. 8) provide some constraints on the timing of pre-extensional exhumation in northwestern Nevada. Broadly, these ages

cluster around 75 Ma, although they range from 80 to 88 Ma in the Black Rock Range to 60 to 70 Ma in the Santa Rosa Range – Bloody Run Hills (table 1 and fig. 8). Modeled time-temperature paths (fig. 10) for these samples indicate cooling from 120° to 60°C in the Late Cretaceous (similar to fig. 9A). Assuming a surface temperature of ~10°C and a typical background arc geothermal gradient (20 – 30°C/km; compare Rothstein and Manning, 2003), samples within 1 km of the Tertiary unconformity cooled through ~60°C at depths of 2 to 3 km, indicating that a significant part of, if not most of, the estimated 5 ± 2 km of post-intrusion erosion took place in the Late Cretaceous (80 – 70 Ma; fig. 10). Samples from the eastern part of the study area (Santa Rosa Range, Bloody Run Hills, and Slumbering Hills; fig. 2) yield slightly younger apparent fission-track ages (table 1; fig. 8) and somewhat more protracted modeled cooling histories (fig. 9B and fig. 10) than samples from the western part of the area (Jackson Mountains, Pine Forest and Black Rock Ranges). Slower or more recent cooling to the east is consistent with more recent exhumation (and higher early to mid-Cenozoic topography) in the eastern part of the study area, where Eocene-Oligocene sedimentary and volcanic rocks are absent, and earlier exhumation (and lower elevations) to the west, where Oligocene and older rocks reach thicknesses exceeding 3 km.

One potential complication with the timing of exhumation is the possibility of Laramide (ca. 75 – 45 Ma) shallow-slab "refrigeration," which could cause a regional drop in the geothermal gradient without significant exhumation (for example; Dumitru, 1990; Dumitru and others, 1991). Many workers consider all or part of the Laramide slab to have been subducted at a shallow angle (for example; Humphreys, 1995), but the depth of the slab and its effect on the temperature of the overlying crust remains uncertain (for example; Saleeby and others, 2003). Depending on the amount and timing of Late Cretaceous cooling, apparent fission-track ages could reflect in part a falling geothermal gradient, with the actual exhumation being younger. However, we interpret Late Cretaceous cooling in northwestern Nevada to represent at least 2 to 3 km of exhumation (of an estimated 5 ± 2 km total), because most shallow samples cooled rapidly and are distinctly older (ca. 88 – 70 Ma; fig. 8) than the main time of presumed shallow-slab subduction (ca. 75 – 45 Ma).

In summary, fission-track data from shallow Oligocene paleodepths in northwestern Nevada define a period of regional cooling in the Late Cretaceous, presumably caused by significant erosion and exhumation at that time. Following the Late Cretaceous cooling event, modeled cooling histories for all shallow fission-track samples indicate a long period of very little erosion, deposition, or tectonism during the Paleocene and Eocene (fig. 10). In northwestern Nevada, shallow (D_u <1 km) fission-track samples were moderately reheated during subsequent Oligocene and Miocene volcanism, while northeastern California (the modern Warner Range, figs. 2 and 3) subsided and became the site of a major volcanoclastic basin by the late Eocene.

(U-Th)/He data from shallow samples (D_u < 1 km).—(U-Th)/He ages from the shallowest exposed levels of plutons (Du <1 km) appear to cluster around 50 Ma, but single-grain ages from individual samples within this interval typically exhibit significant variability, exceeding analytical uncertainties (table 1, fig. 8). For example, two grains from sample BL7 in the Black Rock Range yielded ages of 59 and 27 Ma (table 1). Fitzgerald and others (2006) reviewed within-sample variability in single-grain (U-Th)/He ages and evaluated a number of potential causes, including differences in grain size, U and/or Th zoning, U and/or Th rich inclusions, *et cetera*. The effects of small grain-to-grain differences in these parameters may be magnified when samples cool slowly through the He PRZ (~40 – 85°C), causing significant spreads in single-grain ages (Meesters and Dunai, 2002; Fitzgerald and others, 2006). Modeled fission-track length patterns from shallow (D_u <1 km) samples in this study indicate that rapid Late Cretaceous cooling was followed by reheating to ~60 to 70°C (see for example,
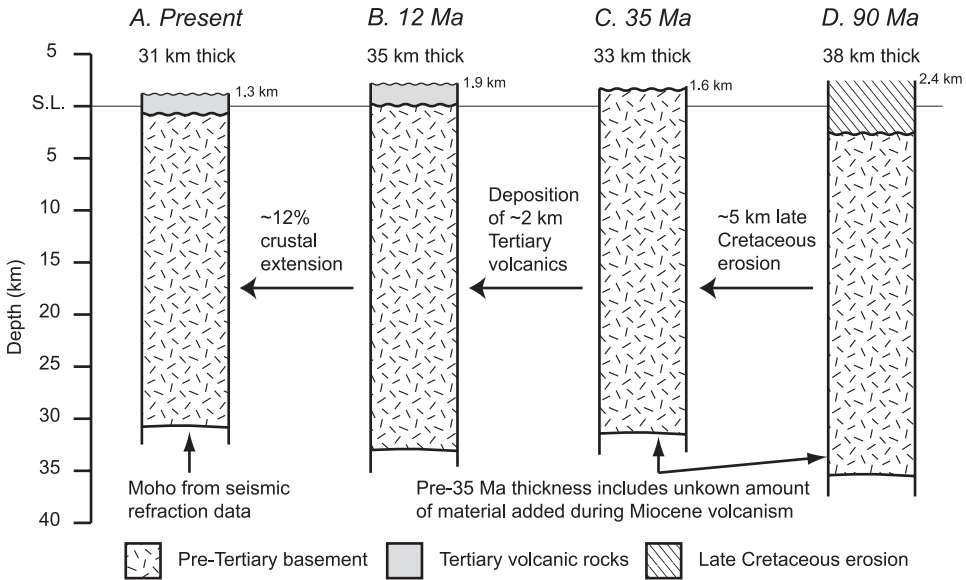
Fig. 11. Schematic crustal columns for northwestern Nevada, showing crustal thickness at different times from the Late Cretaceous to the present as inferred from geologic, geophysical, and thermochronologic data discussed in the text. Surface elevations are calculated assuming isostatic balance of paleo-crustal columns relative to the modern crustal column. All crust is assumed to have a uniform density of 2.8 g/cc, above a mantle with a density of 3.3 g/cc. S.L. is sea level.

fig. 9A) during later burial beneath the overlying Tertiary volcanic section. These temperatures are not hot enough to significantly affect fission-track ages, but are well within the He PRZ. We therefore interpret the older (U-Th)/He ages to represent partial loss of accumulated He during later reheating, with minor physical differences between grains leading to variations in observed ages. For example, modeled fission-track data from sample BL5 in the Black Rock Range indicate rapid cooling through the He PRZ to <60°C at 85 to 90 Ma, followed by reheating to ~65°C during burial beneath Miocene volcanic rocks (fig. 9A). In the absence of later reheating, this sample should yield a consistent (U-Th)/He age of 85 to 90 Ma, but instead yields ages of 65 and 49 Ma. Two single-grain ages per sample are not sufficient to determine a specific cause for the inter-grain variability in our samples, but the observed variability does appear to be compatible with the cooling history derived from the geologic and fission track data.

Pre-Extensional Crustal Thickness

The relatively low magnitude of supracrustal extension in northwestern Nevada allows us to place good constraints on the pre-extensional crustal thickness. Drawing on the available geologic, geophysical, and thermochronologic data, we present a schematic illustration of the crustal thickness in northwestern Nevada from the Late Cretaceous to the present (fig. 11). The modern thickness and velocity structure of the crust in our study area is well-constrained by seismic refraction data collected by Stanford University in 2004 (Lerch and others, 2005a; experiment location shown in fig. 2). These data document an ~31 km thick crust beneath the eastern half of the study area in northwestern Nevada that thickens to about ~36 km in northern California (west of the Warner Range, fig. 2).

To estimate the pre-extensional crustal thickness, we assume homogenous thinning of the crust by ductile flow of the lower crust concurrent with ~13 percent

documented extension in the upper crust in the eastern half of the study area (the 12% figure given in a previous section is for the entire area shown in fig. 2). The present ~31 km thick crust (fig. 11A) in northwestern Nevada was therefore on the order of ~35 km thick prior to the onset of extension at 12 Ma (fig. 11B), in good agreement with the modern ~36 km thickness of the unextended crust just west of the Basin and Range in northern California (Lerch and others, 2005a). Allowing for the deposition of about 2 km of 35 to 15 Ma volcanic rocks implies the crust was about 33 km thick at the end of the Eocene (fig. 11C). Seismic velocity modeling of the crust in northwestern Nevada (Lerch and others, 2005a) does not show a prominent high velocity (>7.0 km/s) layer at the base of crust comparable to the one documented to the south of our study area, where Catchings (1992) interpreted seismic refraction data to represent up to 4 to 7 km of Tertiary magmatic underplating. Although it is possible that the modern crust in northwestern Nevada does include a few km of material added during Tertiary magmatism (Lerch and others, 2005a), we do not include it in our estimates of crustal thickness since the exact amount is not known. Pre-Eocene crustal thickness estimates (figs. 11C and D) therefore do not account for this material (if present) and should thus be considered maximum values. Finally, restoring about 5 km of material eroded during the Late Cretaceous yields a Late Cretaceous crust that was ~38 km thick at most (fig. 11D).

At ~38 km, the early Cenozoic crust in northwestern Nevada was significantly thinner than the pre-extensional, early Cenozoic crust in central and eastern Nevada, which is thought to have been thickened in the hinterland of the Cretaceous Sevier thrust belt (fig. 3; for example; DeCelles and and Coogan, 2006). By restoring Basin and Range extension and assuming homogenous crustal thinning, different workers have estimated pre-extensional crustal thicknesses for central Nevada ranging from 45 km (Smith and others, 1991) to >50 km (Coney and Harms, 1984), with the axis of thickest crust along the modern Nevada-Utah border. Recent studies of the southern Sierra Nevada (south of Reno; fig. 1) have also argued for thick (~75 km) early Cenozoic crust on the basis of xenolith data suggesting the presence of a thick mafic root beneath the granitic batholith from the Late Cretaceous to the late Miocene (for example; Ducea, 2001; Saleeby and others, 2003). Paleoelevation studies utilizing both fossil flora (Wolfe and others, 1998) and stable isotopic data (Horton and others, 2004) have argued for high (3 km) regional elevations in central Nevada (near Elko, fig. 1) and the southern Sierra Nevada from the Eocene to the Miocene, consistent with a thicker early-mid Cenozoic crust in these areas. On the basis of oxygen isotopic analysis of a single sample from Virgin Valley (fig. 2), Horton and others (2004) suggest elevations of ~2 km in northwestern Nevada at 16 Ma, slightly higher than modern elevation of ~1.6 km, but lower than the >3 km they suggest for Elko in the early Miocene. Thus, although there is ample evidence that the crust in regions to the south and east of our study area was significantly thicker (>45 km) during the early-mid Cenozoic, we find no reason to infer that the crust in northwestern Nevada was thicker than ~38 to 33 km during this time. If this is true, it means that the modern ~31 km thick crust in this region was largely inherited from an already thin crust, rather than formed during large-magnitude extension (>50%) of an initially thicker crust (>45–50 km) like the modern Basin and Range crust in central Nevada.

APPENDICES

Appendix A: (U-Th)/He Analytical Procedures

The majority of apatite (U-Th)/He analyses (64) were performed at Yale University; an additional 10 analyses were done at Stanford University. Both laboratories use very similar procedures; the following description of the Yale laboratory applies to Stanford except where specifically noted. Dated apatite grains were hand-picked from prepared mineral concentrates with a high-power (160x) stereo-zoom microscope with cross-polarization for screening inclusions. Individual crystals selected for analysis were digitally photographed and measured in at least 2 different orientations for alpha-ejection correction. Crystals were loaded into 1mm Pt foil tubes, which were loaded into copper or stainless steel planchets and heated with a laser (Nd-YAG at Yale; Argon-ion at Stanford) for 3 minutes at 1–5 W. ^{4}He blanks (0.05–0.1 fmol ^{4}He) were determined by heating empty foil packets using the same procedure.

Gas liberated from samples was processed by: 1) spiking with ~4pmol of ^{3}He, 2) cryogenic concentration at 16K on a charcoal trap (10K at Stanford) and purification by release at 37K, and 3) measurement of ^{4}He/^{3}He ratios (corrected for HD and H$_3$ by monitoring H$^+$) on a quadrapole mass spectrometer. All ratios were referenced to multiple same-day measured ratios and known volumes of ^{4}He standards processed in the same way. After degassing, samples were retrieved from the laser cell, spiked with calibrated ^{229}Th and ^{233}U solution, and dissolved *in-situ* from Pt tubes in ~30% HNO$_3$ (~70% at Stanford) in teflon vials. Each batch of samples was prepared with a series of acid blanks and spiked normals to check the purity and calibration of the reagents and spikes. At Yale, spiked solutions were analyzed as 0.5 mL of ~1.5 ppb U-Th solutions by isotope dilution on a Finnigan Element2 ICP-MS. At Stanford, spiked solutions were analyzed as 0.5 mL of 5 to 20 ppb U-Th solutions by isotope dilution on a Finnigan Element ICP-MS at the University of California, Santa Cruz.

Alpha-ejection was corrected using the method of Farley and others (1996) and Farley (2002). Replicate analyses of Durango apatite (31.44 ± 0.18 Ma; McDowell and others, 2005) during the period of these analyses yielded an age of 32.8 ± 1.1 (2σ, *n* = 3) at Yale, and 31.2 ± 1.3 (2σ, *n* = 6) at Stanford. On the basis of these and other laboratory standards, we estimate an analytical uncertainty of 7% on apatite analyses (for example; Reiners and others, 2003).

TABLE A1

(U-Th)/He analytical data (*denotes samples analyzed at Stanford University; all other samples analyzed at Yale University)

Sample number		Corrected Age ±2σ (Ma)	Ft	Radius (mm)	Mass (mg)	U (ppm)	Th (ppm)	U/Th	He (nmol/g)		Corrected Age ±2σ (Ma)	Ft	Radius (mm)	Mass (mg)	U (ppm)	Th (ppm)	U/Th	He (nmol/g)
JC00-PF1	a	4.8±0.3	0.84	84	13.8	17.9	25.6	0.7	0.5	b	5.6±0.3	0.83	75	12.8	9.0	18.0	0.5	0.3
JC01-PF2	a	5.2±0.3	0.77	57	5.4	9.2	19.0	0.5	0.3	b	6.3±0.4	0.70	42	2.1	14.1	18.8	0.7	0.4
JC01-PF3	a	5.2±0.3	0.77	56	5.9	12.0	22.5	0.5	0.4	b	6.3±0.4	0.79	60	7.6	14.4	27.2	0.5	0.6
JC01-PF4	a	6.6±0.4	0.85	89	18.0	8.7	18.7	0.5	0.4	b	6.8±0.4	0.82	79	9.7	14.5	16.8	0.9	0.6
JC01-PF5	a	7.6±0.5	0.76	55	6.6	24.6	51.0	0.5	1.1	b	6.4±0.4	0.87	111	25.9	7.7	18.0	0.4	0.4
JC01-PF6	a	6.6±0.4	0.80	75	9.7	10.4	19.7	0.5	0.4	b	7.4±0.4	0.79	66	9.3	8.3	18.7	0.4	0.4
JC01-PF7	a	7.4±0.4	0.82	73	12.3	16.1	21.8	0.7	0.7	b	7.7±0.5	0.82	77	9.7	7.3	18.6	0.4	0.4
JC01-PF8	a	8.3±0.5	0.79	63	5.7	6.8	17.7	0.4	0.4	b	8.9±0.5	0.74	54	3.7	8.1	17.3	0.5	0.4
JC01-PF9	a	9.9±0.6	0.85	95	16.1	17.4	30.7	0.6	1.1	b	10.4±0.6	0.71	44	2.5	48.9	30.0	1.6	2.2
JC01-PF10	a	10.1±0.6	0.77	57	4.6	28.3	52.2	0.5	1.7	b	9.2±0.6	0.74	51	4.2	28.1	53.2	0.5	1.5
JC01-PF11	a	12.2±0.7	0.80	72	8.8	34.2	63.2	0.5	2.5	b	12.6±0.8	0.76	59	5.4	36.1	70.4	0.5	2.7
JC01-PF12	a	19.9±1.2	0.81	73	7.8	34.1	59.3	0.6	4.1	b	19.8±1.2	0.79	69	5.3	27.7	53.6	0.5	3.4
JC01-PF13	a	51.8±3.1	0.71	45	3.5	44.8	61.3	0.7	11.7	b	46.9±2.8	0.76	60	5.3	43.1	72.4	0.6	11.5
JC02-PF48	a	3.6±0.2	0.87	106	24.9	33.3	69.1	0.5	0.8	b	3.0±0.2	0.82	74	10.8	24.6	54.0	0.5	0.5
JC02-PF47	a	3.8±0.4	0.68	43	1.4	7.5	4.4	1.7	0.1	b	5.4±0.3	0.70	45	1.9	9.8	7.2	1.4	0.2
JC02-JM2	a	6.7±0.4	0.73	48	2.9	65.3	61.8	1.1	2.1	b	6.6±0.4	0.67	39	1.4	68.3	70.8	1.0	2.0
JC02-BC2	a	154.4±9.5	0.66	37	1.5	0.9	16.7	0.1	2.5	b	49.9±3.0	0.62	34	1.3	7.2	15.7	0.5	1.8
JC02-BC3	a	47.8±2.9	0.72	46	3.5	5.3	13.2	0.4	1.5	b	40.1±2.4	0.74	53	4.3	9.2	20.1	0.5	2.2
JC02-BC4	a	47.6±2.9	0.68	39	2.5	6.0	11.8	0.5	1.5	b	44.1±2.6	0.72	47	3.4	7.1	11.5	0.6	1.6
JC00-SR4	a	50.8±3	0.79	63	5.7	10.7	13.9	0.8	3.0	b	50.9±3.1	0.76	56	6.6	7.8	13.6	0.6	2.3
JC00-SR9	a	33.2±2	0.71	42	2.9	5.2	10.4	0.5	1.0	b	41.6±2.5	0.70	46	2.4	13.1	11.2	1.2	2.4
JC00-SR13	a	16.3±1.0	0.59	31	1.0	13.2	14.0	0.9	0.8	b	26.3±1.6	0.65	35	2.2	10.8	15.7	0.7	1.3
JC00-SR15	a	17.4±1.0	0.72	45	5.0	8.7	13.5	0.6	0.8	b	21.4±1.3	0.76	52	4.7	8.6	16.5	0.5	1.1
JC00-SR22	a	8.8±0.5	0.72	49	2.4	68.7	25.2	2.7	2.6	b	8.9±0.5	0.76	64	3.3	21.9	11.9	1.8	0.9
JC00-SR29	a	11.7±2.0	0.73	53	2.2	0.9	1.3	0.6	0.1	b	14.8±3.9	0.55	29	0.4	5.2	6.1	0.8	0.3
JC00-SR49	a	13.7±1.2	0.62	33	0.9	7.5	10.2	0.7	0.4	b	40.9±7.2	0.63	32	1.2	0.6	7.0	0.1	0.3
JC01-SR50	a	11.1±0.7	0.77	58	4.3	26.0	11.7	2.2	1.3	b	13.9±0.8	0.70	43	1.9	44.0	13.7	3.2	2.5
JC03-BL5	a	64.6±3.9	0.75	53	5.9	41.2	59.1	0.7	14.4	b	47.8±2.9	0.75	52	5.2	74.7	107.4	0.7	19.1
JC03-BL6	a	48.9±2.9	0.75	56	4.4	47.9	82.6	0.6	13.1	b	608±36.5	0.70	44	3.2	34.6	54.9	0.6	111.9
JC03-BL7	a	58.5±3.5	0.78	63	7.7	102.9	76.3	1.3	29.8	b	27.0±1.6	0.76	54	6.1	120.9	87.7	1.4	15.5
JC04-WR122	a	3.0±0.8	0.71	43	2.8	3.4	5.1	0.7	0.1	b	2.0±0.1	0.82	76	12.9	3.0	6.9	0.4	0.0
JC04-WR104	a	3.3±0.2	0.69	42	2.4	20.5	29.3	0.7	0.3	b	3.2±0.2	0.78	61	7.2	16.7	25.9	0.6	0.3
JC02-BR1*	a	57.3±4.3	0.77	65	9.4	10.1	21.0	0.5	3.9	b	47.7±3.3	0.79	74	12.7	6.8	14.2	0.5	2.3
JC02-BR2*	a	30.6±1.8	0.82	84	21.3	11.5	17.3	0.7	2.3	b	36.6±2.0	0.84	94	29.1	12.6	19.5	0.6	3.1
JC02-BR3*	a	36.1±2.5	0.81	80	16.6	10.4	18.1	0.6	2.6	b	36.5±2.6	0.78	68	9.4	15.0	21.5	0.7	3.4
JC02-SH1*	a	63.7±2.9	0.81	77	14.2	10.0	6.0	1.7	3.5	b	61.6±2.5	0.79	72	15.9	17.2	7.9	2.2	5.6
JC02-SH2*	a	81.3±8.5	0.74	58	6.2	20.5	103.1	0.2	16.0	b	57.8±5.1	0.73	55	4.2	11.4	24.3	0.5	4.3

All samples were prepared and analyzed by J. P. Colgan at Stanford University. Apatite concentrates were prepared using standard mineral separation techniques, including crushing, grinding, Frantz magnetic separation, and heavy liquids. Apatites were mounted in epoxy on glass slides and ground and polished by hand. Polished grain-mounts were etched for 20 s in 5N nitric acid at 22°C and affixed to muscovite external detectors. Samples and external detectors were stacked single-file in plastic reactor cans and irradiated in well thermalized positions of the Oregon State University TRIGA reactor. CN5 dosimetry glasses with muscovite external detectors were used as neutron flux monitors (3 per can). After irradiation, external detectors were etched in 48 percent HF.

Tracks were counted with a Zeiss Axioskop microscope with a 100x air objective, 1.25x tube factor, 10x eyepieces, and transmitted light with supplementary reflected light as needed. External detector prints were located with Kinetek automated scanning stage (Dumitru, 1993). Only grains with c axes subparallel to the slide plane were dated. Ages calculated using zeta calibration factor of 367.6 ± 5.0 (for example; Hurford and Green, 1983). Ages reported are the fission-track central age of Galbraith and Laslett (1993). Confined track lengths were measured only in apatite grains with c axes subparallel to slide plane; only horizontal tracks were measured (within $\pm 5 - 10°$), following protocols of Laslett and others (1982). Lengths were measured with computer digitizing tablet and drawing tube, calibrated against a stage micrometer (Dumitru, 1993). Confined track lengths were measured along with angles of tracks to the grains' c-axes, following the protocols of Ketcham and others (1999, 2000). Confined tracks hosted by surface tracks and by cleavage surfaces were both measured.

Age calculations were done with an Excel® program by J. Colgan. Length models were generated using the AFTSolve program by Ketcham and others (2000), using the annealing model of Ketcham and others (1999). Only samples with greater than 20 measured lengths were modeled and lengths were not c-axis projected. For each model, 1000 paths were calculated, paths were split 3 times, and all segments were monotonic. AFTSolve cannot model zero-age grains; therefore zero-age grains were deleted from some young samples prior to modeling. Quantitative information can still be obtained about the cooling rate of these samples, but the modeled age will be slightly too old. Modeled time-temperature paths for all samples are presented in Colgan (ms, 2005).

Zircon concentrates were prepared at Stanford University and handpicked under a binocular microscope to ensure purity and freedom from cracks, inclusions, or obvious alteration. At the Stanford - U.S.G.S. Micro Analytical Center (SUMAC), the selected grains were mounted in epoxy with the laboratory standard R33 (419 Ma; Black and others, 2004) and polished with diamond compound to expose the mid-points of the crystals. Polished grain mounts were imaged in reflected light with an optical microscope, gold-coated, and imaged in cathodoluminescence (CL) mode with a JEOL 5600 scanning electron microscope.

The SHRIMP-RG ion microprobe at SUMAC was operated with an O_2^- primary ion beam varying from 4 to 6 nA, which produced a spot with a diameter of ~ 20 to 30 μm and a depth of 1 to 2 μm on the target zircons. Eleven peaks were measured sequentially for 10 min with an ETP electron multiplier (Zr_2O, ^{204}Pb, ^{206}Pb, ^{207}Pb, ^{208}Pb, ^{238}U, ThO, UO, ErO, YbO, and HfO). Data was reduced following the methods described by Ireland and Williams (2003), using the SQUID and IsoPlot programs of Ludwig (2001, 2003). Analytical data is presented in table C1. Inverse-concordia diagrams for each sample are shown in figure C1.

Table B1

Fission-track counting and age data

Sample number	Irradiation number	No xls	Spontaneous		Induced		P(χ^2) (%)	Dosimeter		Age ± 1σ (Ma)	No T.L.	Track L. (μm ± S.D.)
			Rho-S	NS	Rho-I	NI		Rho-D	ND			
JC00-PF1	SU055-19	35	0.0326	63	1.0069	1944	44.7	1.4729	3877	8.8 ± 1.1	22	13.85 ± 0.45
JC01-PF2	SU058-01	36	0.0597	130	1.3635	2969	36.2	1.3743	4065	11.0 ± 1.0	31	13.31 ± 0.28
JC01-PF3	SU058-02	35	0.0386	113	1.0563	3095	25.3	1.3818	4065	9.3 ± 1.0	21	13.83 ± 0.37
JC01-PF4	SU058-03	35	0.0485	156	1.1313	3638	17.2	1.3818	4065	10.8 ± 1.0	11	14.05 ± 0.51
JC01-PF5	SU058-04	35	0.0479	139	1.1090	3217	48.7	1.3967	4065	11.1 ± 1.0	43	14.03 ± 0.21
JC01-PF6	SU058-05	35	0.0631	179	1.3521	3838	56.8	1.3967	4065	12.0 ± 1.0	16	13.76 ± 0.38
JC01-PF7	SU058-06	35	0.0631	146	1.1713	2710	72.5	1.4116	4065	14.0 ± 1.2	122	13.08 ± 0.22
JC01-PF8	SU058-07	35	0.0949	208	0.9945	2179	15.8	1.4116	4065	24.7 ± 1.9	25	12.10 ± 0.31
JC01-PF9	SU058-08	35	0.2896	598	2.2516	4649	15.4	1.4264	4065	33.7 ± 1.8	150	12.57 ± 0.14
JC01-PF10	SU058-09	35	0.2697	474	2.1342	3751	34.9	1.4264	4065	33.1 ± 1.7	153	12.67 ± 0.11
JC01-PF11	SU058-10	30	0.2920	578	3.5464	7019	77.8	1.4413	4065	21.8 ± 1.1	150	14.67 ± 0.12
JC01-PF12	SU058-12	30	0.4287	741	2.8998	5012	35.2	1.4488	4065	39.2 ± 1.9	153	13.43 ± 0.10
JC01-PF13	SU058-13	31	1.1561	2223	3.7185	7150	31.2	1.4637	4065	83.1 ± 2.8	150	13.61 ± 0.09
JC01-PF14	SU058-14	25	1.8266	3118	6.5541	11188	0.1	1.4637	4065	75.0 ± 2.4	134	13.52 ± 0.09
JC02-PF44	SU059-06	23	1.6828	849	5.4526	2751	18.9	1.4040	4095	79.3 ± 4.0	150	12.93 ± 0.09
JC02-PF47	SU059-07	35	0.0425	60	1.6103	2273	1.1	1.4125	4095	7.3 ± 1.0		*no lengths*
JC02-PF48	SU059-08	35	0.0754	110	2.8126	4104	8.8	1.4125	4095	7.0 ± 0.7	63	14.06 ± 0.14
JC00-SR4	SU058-15	35	0.3167	904	1.1107	3170	47.3	1.4790	4065	77.1 ± 3.3	150	13.89 ± 0.12
JC00-SR9	SU055-11	31	0.3996	787	1.4019	2761	0.0	1.3733	3877	70.3 ± 4.5	150	13.30 ± 0.13
JC00-SR13	SU058-16	29	0.2556	668	1.2556	3281	7.9	1.4790	4065	54.0 ± 3.0	150	13.82 ± 0.14
JC00-SR15	SU055-13	36	0.3568	727	1.7035	3471	41.0	1.4065	3877	52.8 ± 2.5	150	13.38 ± 0.12
JC00-SR17	SU055-14	24	0.1340	211	3.5382	5572	8.3	1.4065	3877	9.6 ± 0.8	8	14.28 ± 0.41
JC00-SR19	SU055-15	21	0.0799	109	2.5593	3493	4.3	1.4286	3877	8.1 ± 0.9	4	12.00 ± 1.25
JC00-SR22	SU055-16	31	0.1584	210	4.9602	6577	82.6	1.4286	3899	8.2 ± 0.6	43	14.01 ± 0.12
JC00-SR29	SU055-17	29	0.0602	102	2.4349	4128	30.1	1.4510	3877	6.4 ± 0.8	22	13.88 ± 0.25
JC02-SR49	SU055-18	30	0.1007	167	1.6299	2703	10.9	1.4510	3877	15.3 ± 1.6	44	13.10 ± 0.29
JC00-SR50	SU058-17	32	0.1098	243	2.7064	5988	0.2	1.4930	4065	11.4 ± 0.9	37	13.85 ± 0.59
JC01-SR51	SU058-18	35	0.1088	195	2.8222	5059	45.7	1.4930	4065	10.5 ± 0.8	28	13.25 ± 0.34
JC01-SR52	SU058-19	27	0.0897	93	1.8827	1951	90.0	1.5080	4065	13.2 ± 1.4	35	13.77 ± 0.31
JC02-BR1	SU059-03	20	0.3232	421	1.1523	1501	93.1	1.3954	4095	71.6 ± 4.2	88	13.62 ± 0.17
JC02-BR2	SU059-04	20	0.3575	570	1.6610	2648	84.9	1.3954	4095	55.0 ± 2.8	152	13.35 ± 0.12
JC02-BR3	SU059-05	15	0.3363	306	2.0112	1830	98.2	1.4040	4095	43.0 ± 2.8	150	11.46 ± 0.20
JC02-SH1	SU059-20	20	0.4708	487	2.0796	2151	70.3	1.4636	4095	60.7 ± 3.3	150	13.90 ± 0.10
JC02-SH2	SU059-21	22	0.4851	415	1.9323	1653	7.3	1.4721	4095	68.1 ± 4.4	150	13.77 ± 0.11
JC02-BC2	SU059-15	20	0.3550	432	1.2809	1559	92.4	1.4465	4095	73.3 ± 4.3	150	13.64 ± 0.11
JC02-BC3	SU059-16	20	0.3035	452	1.1637	1733	3.4	1.4465	4095	70.5 ± 5.2	131	12.84 ± 0.11
JC02-BC4	SU059-17	25	0.3565	506	1.2591	1787	69.4	1.4550	4095	75.3 ± 4.1	99	13.46 ± 0.13
JC02-JM1	SU059-01	25	1.1406	591	3.5126	1820	88.1	1.3869	4065	82.3 ± 4.3	150	14.01 ± 0.11
JC02-JM2	SU059-02	13	0.2644	64	5.7425	1390	96.7	1.3869	4095	11.7 ± 1.5	71	14.15 ± 0.15
JC02-PM1	SU059-09	20	0.7487	754	2.8647	2885	17.4	1.4210	4095	67.9 ± 3.1	151	13.45 ± 0.08
JC02-PM3	SU059-11	10	0.7416	93	2.9426	369	0.0	1.3818	4065	73.2 ±16.3		*no lengths*
JC02-PM4	SU059-12	15	0.1232	91	2.0493	1514	32.3	1.4295	4095	15.8 ± 1.8	31	12.71 ± 0.47
JC03-BL5	SU060-07	12	2.2044	1500	6.4896	4416	66.8	1.4030	4056	87.0 ± 3.2	150	13.89 ± 0.07
JC03-BL6	SU060-08	12	1.3656	1285	4.3879	4129	6.3	1.4030	4056	80.2 ± 3.7	150	13.85 ± 0.07
JC03-BL7	SU060-09	8	2.5978	1697	8.5848	5608	10.1	1.4207	4056	78.7 ± 3.2	150	14.06 ± 0.07
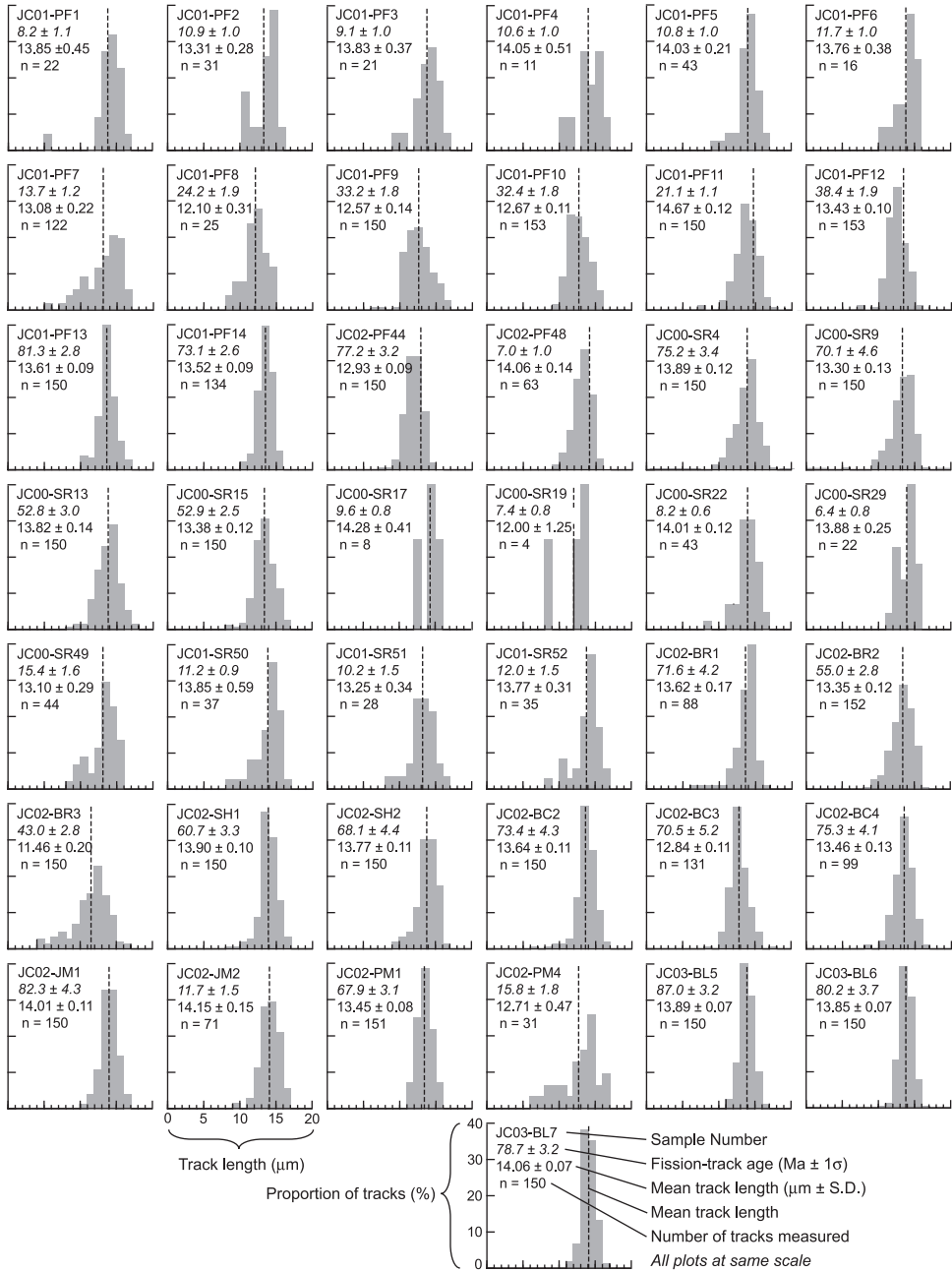
Figure B1

TABLE C1

U-Pb SHRIMP analytical data

| Spot name	comm 206 (%)	U (ppm)	Th (ppm)	^{232}Th/^{238}U	^{206}Pb/^{238}U Age* (Ma, ±1σ)	Total ^{238}U/^{206}Pb (± % err)	Total ^{207}Pb/^{206}Pb (± % err)
JC00-SR4: Santa Rosa Range							
SR4-1	0.36	421	143	0.35	97.9 ± 1.7	65.1 ± 1.7	0.0508 ± 4.0
SR4-2	0.28	316	94	0.31	102.8 ± 1.8	62.1 ± 1.8	0.0503 ± 4.4
SR4-3	-0.14	305	90	0.30	106.8 ± 1.9	59.9 ± 1.8	0.0470 ± 4.6
SR4-4	-0.03	247	100	0.42	104.4 ± 2.0	61.3 ± 1.9	0.0478 ± 5.1
SR4-5	0.05	377	148	0.40	106.0 ± 1.8	60.3 ± 1.7	0.0486 ± 4.1
SR4-6	0.29	376	142	0.39	99.5 ± 1.7	64.1 ± 1.7	0.0503 ± 4.1
SR4-7	-0.03	400	140	0.36	106.2 ± 1.8	60.2 ± 1.7	0.0479 ± 4.0
SR4-8	-0.13	484	221	0.47	104.7 ± 1.7	61.2 ± 1.6	0.0471 ± 3.8
SR4-9	-0.07	388	175	0.46	103.5 ± 1.7	61.8 ± 1.7	0.0475 ± 4.0
SR4-10	-0.24	376	135	0.37	107.6 ± 1.8	59.5 ± 1.7	0.0463 ± 4.2
SR4-11	0.14	507	255	0.52	105.4 ± 1.7	60.6 ± 1.6	0.0493 ± 3.4
SR4-12	0.20	629	131	0.22	102.8 ± 1.6	62.1 ± 1.5	0.0497 ± 3.1
JC02-BR2: Bloody Run Hills							
BR2-1	0.21	336	104	0.32	96.6 ± 1.7	66.1 ± 1.8	0.0496 ± 4.4
BR2-2	0.49	122	69	0.58	92.9 ± 2.3	68.5 ± 2.4	0.0517 ± 7.3
BR2-3	0.06	675	179	0.27	102.4 ± 1.5	62.4 ± 1.5	0.0486 ± 3.0
BR2-4	0.09	1317	545	0.43	103.4 ± 1.4	61.8 ± 1.4	0.0488 ± 2.2
BR2-5	0.40	465	233	0.52	98.1 ± 1.6	64.9 ± 1.6	0.0511 ± 3.8
BR2-6	0.01	744	294	0.41	99.1 ± 1.5	64.6 ± 1.5	0.0481 ± 3.0
BR2-7	-0.03	268	99	0.38	96.8 ± 1.8	66.1 ± 1.9	0.0477 ± 5.0
BR2-8	-0.25	785	327	0.43	97.0 ± 1.5	66.1 ± 1.5	0.0460 ± 4.0
BR2-9	0.59	381	108	0.29	92.3 ± 1.6	68.9 ± 1.7	0.0525 ± 4.1
BR2-10	0.13	550	148	0.28	97.8 ± 1.5	65.3 ± 1.6	0.0490 ± 3.4
JC02-SH2: Slumbering Hills							
SH2-1	-0.10	451	88	0.20	113.4 ± 1.8	56.4 ± 1.6	0.0475 ± 3.5
SH2-2	0.18	3432	949	0.29	115.9 ± 1.5	55.0 ± 1.3	0.0498 ± 1.2
SH2-3	-0.08	523	139	0.27	114.0 ± 1.8	56.1 ± 1.5	0.0477 ± 3.3
SH2-4	-0.57	500	340	0.70	119.9 ± 1.9	53.6 ± 1.6	0.0439 ± 3.5
SH2-5	0.04	1260	314	0.26	117.3 ± 1.6	54.5 ± 1.4	0.0487 ± 2.1
SH2-6	0.41	559	167	0.31	115.0 ± 1.8	55.3 ± 1.5	0.0516 ± 3.0
SH2-7	0.48	599	176	0.30	110.1 ± 1.7	57.8 ± 1.5	0.0520 ± 3.1
SH2-8	-0.04	594	180	0.31	113.7 ± 1.7	56.2 ± 1.5	0.0479 ± 3.1
SH2-9	0.12	9604	1328	0.14	117.5 ± 1.5	54.3 ± 1.3	0.0494 ± 0.7
SH2-10	0.32	413	228	0.57	101.4 ± 1.7	62.9 ± 1.6	0.0506 ± 3.8
JC02-BC2: Bilk Creek Mountains							
BC2-1	-0.10	222	77	0.36	101.4 ± 1.9	63.1 ± 1.9	0.0473 ± 5.3
BC2-2	0.31	65	22	0.35	101.8 ± 3.0	62.7 ± 2.9	0.0505 ± 9.4
BC2-3	0.19	55	23	0.43	101.3 ± 3.2	63.0 ± 3.1	0.0496 ± 10.3
BC2-4	0.02	634	258	0.42	109.0 ± 1.6	58.6 ± 1.5	0.0484 ± 3.0
BC2-5	0.08	112	55	0.51	106.2 ± 2.5	60.2 ± 2.3	0.0488 ± 7.3
BC2-6R	0.45	166	45	0.28	101.0 ± 2.1	63.0 ± 2.1	0.0516 ± 5.9
BC2-7	0.20	52	15	0.30	104.4 ± 3.4	61.1 ± 3.2	0.0497 ± 10.7
BC2-8	-0.28	49	17	0.36	104.2 ± 3.5	61.5 ± 3.2	0.0459 ± 19.0
BC2-9	0.78	137	49	0.37	103.4 ± 2.3	61.3 ± 2.2	0.0542 ± 6.2
JC03-BL6: Black Rock Range							
BL6-1	-0.22	594	365	0.63	113.8 ± 1.7	56.3 ± 1.5	0.0466 ± 3.1
BL6-2	-0.09	569	318	0.58	113.5 ± 2.1	56.4 ± 1.8	0.0476 ± 3.2
BL6-3	-0.18	441	279	0.65	112.6 ± 1.8	56.9 ± 1.6	0.0468 ± 3.6
BL6-4	0.28	554	312	0.58	110.1 ± 1.7	57.9 ± 1.5	0.0504 ± 3.1
BL6-5	0.45	607	308	0.52	111.3 ± 1.7	57.2 ± 1.5	0.0518 ± 3.0
BL6-6	0.01	731	415	0.59	111.1 ± 1.6	57.5 ± 1.5	0.0483 ± 2.8
BL6-7	0.13	422	257	0.63	111.0 ± 1.8	57.5 ± 1.6	0.0492 ± 3.6
BL6-8	0.56	481	270	0.58	112.2 ± 1.8	56.6 ± 1.6	0.0527 ± 3.3
BL6-9	-0.11	675	390	0.60	114.5 ± 1.7	55.9 ± 1.5	0.0474 ± 2.9
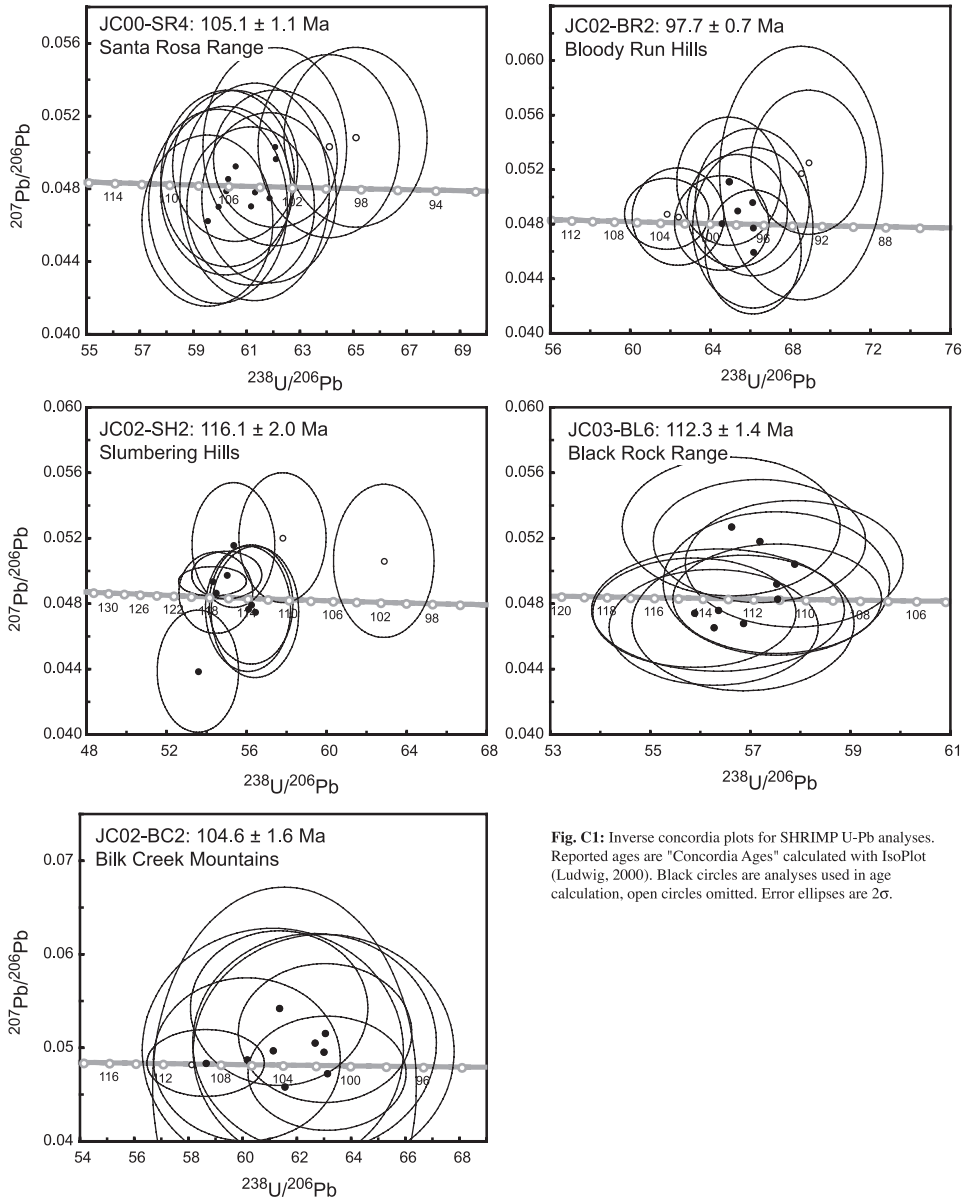
Fig. C1: Inverse concordia plots for SHRIMP U-Pb analyses. Reported ages are "Concordia Ages" calculated with IsoPlot (Ludwig, 2000). Black circles are analyses used in age calculation, open circles omitted. Error ellipses are 2σ.

Figure C1

REFERENCES

Ague, J. J., and Brimhall, G. H., 1988, Magmatic arc asymmetry and distribution of anomalous plutonic belts in the batholiths of California: Effects of assimilation, crustal thickness, and depth of crystallization: Geological Society of America Bulletin, v. 100, p. 912–927.

Argus, D. F., and Gordon, R. G., 2001, Present tectonic motion across the Coast Ranges and San Andreas fault system in central California: Geological Society of America Bulletin, v. 113, p. 1580–1592.

Armstrong, P. A., Ehlers, T. A., Chapman, D. S., Farley, K. A., and Kamp, P. J., 2003, Exhumation of the central Wasatch Mountains, Utah: 1. Patterns and timing of exhumation deduced from low-temperature thermochronology data: Journal of Geophysical Research, v. 108, B3, 2172, doi:10.1029/2001JB001708.

Atwater, T., and Stock, J., 1998, Pacific-North America plate tectonics of the Neogene southwestern United States: An update: International Geology Review, v. 40, p. 375–402.

Barton, M. D., and Hanson, R. B., 1989, Magmatism and the development of low-pressure metamorphic belts: Implications from the western United States and thermal modeling: Geological Society of America Bulletin, v. 101, p. 1051–1065.

Black, L. P., Kamo, S. L., Allen, C. M., Davis, D. W., Aleinikoff, J. N., Valley, J. W., Mundil, R., Campbell, I. H., Korsch, R. J., Williams, I. S., and Foudoulis, C., 2004, Improved $^{206}Pb/^{238}U$ microprobe geochronology by the monitoring of a trace-element-related matrix effect: SHRIMP, ID-TIMS, ELA-ICP-MS, and oxygen isotope documentation for a series of zircon standards: Chemical Geology, v. 205, p. 115–140.

Blackwell, D. D., and Steele, J. L., 1992, Geothermal Map of North America: Geological Society of America, DNAG Map no. 006, 1992.

Blackwell, D. D., Steele, J. L., and Carter, L. S., 1991, Heat flow patterns of the North American continent: A discussion of the DNAG geothermal map of North America, *in* Slemmons, D. B., Engdahl, E. R., and Blackwell, D. D., editors, Neotectonics of North America: Geological Society of America DNAG Decade Map, v. 1, p. 423-437.

Brueseke, M. E., Hart, W. K., and Heizler, M. T., 2006, Diverse mid-Miocene silicic volcanism associated with the Yellowstone-Newberry thermal anomaly: Bulletin of Volcanology, special issue: Petrogenesis and volcanology of anorogenic rhyolites in the northwest intermountain USA.

Carmichael, I. S. E., Lange, R. A., Hall, C. M., and Renne, P. R., 2006, Faulted and tilted Pliocene olivine tholeiite lavas near Alturas, NE California, and their bearing on the uplift of the Warner Range: Geological Society of America Bulletin, v. 118, p. 1196–1211.

Carter, T. J., Kohn, B. P., Foster, D. A., Gleadow, A. J. W., and Woodhead, J. D., 2006, Late-stage evolution of the Chemehuevi and Sacramento detachment faults from apatite (U-Th)/He thermochronometry – Evidence for mid-Miocene accelerated slip: Geological Society of America Bulletin, v. 118, p. 689–709.

Cashman, P. H., and Fontaine, C. A., 2000, Strain partitioning in the northern Walker Lane, western Nevada and northeastern California: Tectonophysics, v. 326, p. 111–130.

Castor, S. B., and Henry, C. D., 2000, Geology, geochemistry, and origin of volcanic rock-hosted uranium deposits in northwestern Nevada and southeastern Oregon, USA: Ore Geology Reviews, v. 16, p. 1–40.

Catchings, R. D., 1992, A relation among geology, tectonics, and velocity structure, western to central Basin and Range: Geological Society of America Bulletin, v. 104, p. 1178–1192.

Christiansen, R. L., and Yeats, R. S., 1992, Post-Laramide geology of the U.S. Cordilleran region, *in* Burchfiel, B. C., Lipman, P. W., and Zoback, M. L., editors, The Cordilleran Orogen: Conterminous U.S.: Boulder, Colorado, Geological Society of America, The Geology of North America, v. G-3, Decade of North American Geology, p. 553–581.

Colgan, J. P., ms, 2005, Timing and magnitude of Basin and Range extension in northwestern Nevada: Palo Alto, California, Stanford University, Ph.D. thesis, 160 p.

Colgan, J. P., Dumitru, T. A., and Miller, E. L., 2004, Diachroneity of Basin and Range extension and Yellowstone hotspot volcanism in northwestern Nevada: Geology, v. 32, p. 121–124.

Colgan, J. P., Dumitru, T. A., Miller, E. L., and McWilliams, M. O., 2006, Timing of Cenozoic volcanism and Basin and Range extension in northwestern Nevada: new constraints from the northern Pine Forest Range: Geological Society of America Bulletin, v. 118, p. 126–139.

Compton, R. R., 1960, Contact metamorphism in Santa Rosa Range, Nevada: Geological Society of America Bulletin, v. 71, p. 1383–1416.

Coney, P. J., and Harms, T. A., 1984, Cordilleran metamorphic core complexes; Cenozoic extensional relics of Mesozoic compression: Geology, v. 12, p. 550–554.

DeCelles, P. G., and Coogan, J. C., 2006, Regional structure and kinematic history of the Sevier fold-and-thrust belt, central Utah: Geological Society of America Bulletin, v. 118, p. 841 864.

Dilles, J. H., and Gans, P. B., 1995, The chronology of Cenozoic volcanism and deformation in the Yerington area, western Basin and Range and Walker Lane: Geological Society of America Bulletin, v. 107, p. 474–486.

Ducea, M. N., 2001, The California arc: Thick granitic batholiths, ecogitic residues, lithospheric-scale thrusting, and magmatic flare-ups: GSA Today, v. 11, p. 4–10.

Duffield, W. A., and McKee, E. H., 1986, Geochronology, structure, and basin-range tectonism of the Warner Range, northeastern California: Geological Society of America Bulletin, v. 97, p. 142–146.

Dumitru, T. A., 1990, Subnormal Cenozoic geothermal gradients in the extinct Sierra Nevada magmatic arc; consequences of Laramide and post-Laramide shallow-angle subduction: Journal of Geophysical Research, v. 95, p. 4925–4941.

—— 1993, A new computer-automated microscope stage system for fission-track analysis: Nuclear Tracks and Radiation Measurements, v. 21, p. 575-580.

—— 2000, Fission-track geochronology in Quaternary geology, *in* Noller, J. S., Sowers, J. M., and Lettis, W. R., editors, Quaternary geochronology: Methods and Applications: American Geophysical Union Reference Shelf, v. 4, p. 131–156.

Dumitru, T. A., Gans, P. B., Foster, D. A., and Miller, E. L., 1991, Refrigeration of the western Cordilleran lithosphere during Laramide shallow-angle subduction: Geology, v. 19, p. 1145–1148.

Egger, A. E., Dumitru, T. A., Miller, E. L., Savage, C. F. I., and Wooden, J. L., 2003, Timing and nature of Tertiary plutonism and extension in the Grouse Creek Mountains, Utah: International Geology Review, v. 45, p. 497–532.

Ehlers, T. A., Willett, S. D., Armstrong, P. A., and Chapman, D. S., 2003, Exhumation of the Central Wasatch Mountains 2: Thermo-kinematics models of exhumation, erosion and low-temperature thermochronometer interpretation: Journal of Geophysical Research, v. 108, 2173, doi:10.1029/2001JB001723.

Farley, K. A., 2000, Helium diffusion from apatite I: General behavior as illustrated by Durango fluorapatite: Journal of Geophysical Research, v. 105, p. 2903–2914.

—— 2002, (U-Th)/He dating: Techniques, calibrations, and applications, *in* Porcelli, D., Ballentine, C. J., and Wieler, R., editors, Noble gases in geochemistry and cosmochemistry: Mineralogical Society of America, Reviews in Mineralogy and Geochemistry, v. 47, p. 819–844.

Farley, K. A., Wolf, R. A., and Silver, L.T., 1996, The effect of long alpha-stopping distances on (U-Th)/He ages: Geochemica et Cosmochemica Acta, v. 60, p. 4223–4229.

Fitzgerald, P. G., Fryxell, J. E., and Wernicke, B. P., 1991, Miocene crustal extension and uplift in southeastern Nevada, constraints from fission-track analysis: Geology, v. 19, p. 1012–1016.

Fitzgerald, P. G., Baldwin, S. L., Webb, L. E., and O'Sullivan, P., 2006, (U-Th)/He data from slowly cooled crustal terranes and the interpretation of intra-sample variations of single crystal apatite ages from vertical profiles: Chemical Geology, v. 225, p. 91–120.

Flesch, L. M., Holt, W. E., Haines, J. A., and Bingming, S., 2000, Dynamics of the Pacific-North American plate boundary in the western United States: Science, v. 287, p. 434–436.

Fliedner, M. M., Klemperer, S. L., and Christensen, N. I., 2000, Three-dimensional seismic model of the Sierra Nevada arc, California, and its implications for crustal and upper mantle composition: Journal of Geophysical Research, v. 105, p. 10,899–10,921.

Foster, D. A., and John, B. E., 1999, Quantifying tectonic exhumation in an extensional orogen with thermochronology: examples from the Basin and Range Province, *in* Ring, U., Brandon, M. T., Lister, G. S., and Willett, S., editors, Exhumation processes: normal faulting, ductile flow, and erosion: London, England, Geological Society Special Publication, 154, p. 356–378.

Foster, D. A., Miller, D. S., and Miller, C. F., 1991, Tertiary extension in the Old Woman Mountains area, California: Evidence from apatite fission-track analysis: Tectonics, v. 10, p. 875–886.

Foster, D. A., Gleadow, A. J. W., Reynolds, S. J., and Fitzgerald, P. Q., 1993, The denudation of metamorphic core complexes and the reconstruction of the Transition Zone, west-central Arizona: constraints from apatite fission-track thermochronology: Journal of Geophysical Research, v. 98, p. 2167-2185.

Galbraith, R. F., and Laslett, G. M., 1993, Statistical models for mixed fission-track ages: Nuclear Tracks and Radiation Measurements, v. 21, p. 459-470.

Gleadow, A. J. W., Duddy, I. R., Green, P. F., and Lovering, J. F., 1986, Confined fission track lengths in apatite; a diagnostic tool for thermal history analysis: Contributions to Mineralogy and Petrology, v. 94, p. 405–415.

Green, P. F., Duddy, I. R., Laslett, G. M., Hegarty, K. A., Gleadow, A. J. W., and Lovering, J. F., 1989, Thermal annealing of fission tracks in apatite: 4. Quantitative modeling techniques and extension to geological time scales: Chemical Geology (Isotope Geoscience Section), v. 79, p. 155–182.

Greene, R. C., 1984, Geologic appraisal of the Charles Sheldon Wilderness Study Area, Nevada and Oregon: U. S. Geological Survey Bulletin 1538-A, scale 1:125,000.

Hammond, W. C., and Thatcher. W., 2005, Northwest Basin and Range tectonic deformation observed with the Global Positioning System, 1999–2003: Journal of Geophysical Research, v. 110, B10405, doi:10.1029/2005JB003678.

Hart, W. K., Carlson, R. W., and Mosher, S. A., 1989, Petrogenesis of the Pueblo Mountains basalt, southeastern Oregon and northern Nevada, *in* Reidel, S. P., and Hooper, P. R., editors, volcanism and tectonism in the Columbia River flood–basalt province: Boulder, Colorado, Geological Society of America, Special Paper 239, p. 367–378.

Hedel, C. W., 1984, Map showing geomorphic and geologic evidence for late Quaternary displacement along the Surprise Valley and associated faults, Modoc County, California: U.S. Geological Survey Miscellaneous Field Studies Map MF-1429, scale 1:62,500.

Henry, C. D., and Perkins, M. E., 2001, Sierra Nevada - Basin and Range transition near Reno, Nevada: two stage development at 12 and 3 Ma: Geology, v. 29, p. 719–722.

Horton, T. W., Sjostrom, D. J., Abruzzese, M. J., Poage, M. A., Waldbauer, J. R., Hren, M., Wooden, J., and Chamberlain, C. P., 2004, Spatial and temporal variation of Cenozoic surface uplift in the Great Basin and Eastern Sierra Nevada: American Journal of Science, v. 304, p. 862–888.

Howard, K. A., 2003, Crustal Structure in the Elko-Carlin Region, Nevada, during Eocene Gold Mineralization: Ruby-East Humboldt Metamorphic Core Complex as a Guide to the Deep Crust: Economic Geology, v. 98, p. 249–268.

Howard, K. A., and Foster, D. A., 1996, Thermal and unroofing history of a thick, tilted Basin and Range crustal section in the Tortilla Mountains, Arizona: Journal of Geophysical Research, v. 101, p. 511–522.

Hudson, J. R., John, D. A., Conrad, J. E., and McKee, E. H., 2000, Style and age of late Oligocene-Early Miocene deformation in the southern Stillwater Range, west-central Nevada: Paleomagnetism, geochronology, and field relations: Journal of Geophysical Research, v. 105, p. 929–954.

Humphreys, E. D., 1995, Post-Laramide removal of the Farallon Slab, Western United States: Geology, v. 23, p. 987–990.

Hurford, A. J., and Green, P. F., 1983, The zeta age calibration in fission-track dating: Chemical Geology, v. 41, p. 285-317.

Jennings, C. W., Strand, R. G., and Rogers, T. H., 1977, Geologic Map of California: California Division of Mines and Geology, scale 1:750,000.

Ireland, T. R., and Williams, I. S., 2003, Considerations in zircon geochronology by SIMS, *in* Hanchar, J. M., and Hoskin, P. W. O., editors, Zircon: Mineralogical Society of America and Geochemical Society, Reviews in Mineralogy and Geochemistry, v. 53, p. 215–241.

Jones, E. A., 1990, Geology and tectonic significance of terranes near Quinn River Crossing, Nevada, *in* Harwood, D. S., and Miller, M. M., editors, Paleozoic and early Mesozoic paleogeographic relations; Sierra Nevada, Klamath Mountains, and related terranes: Boulder, Colorado, Geological Society of America Special Paper 255, p. 239–253.

Ketcham, R. A., Donelick, R. A., and Carlson, W. D., 1999, Variability of apatite fission-track annealing kinetics. 3. Extrapolation to geological time scales: American Mineralogist, v. 84, p. 1235–1255.

Ketcham, R. A., Donelick, R. A., and Donelick, M. B., 2000, AFTSolve: A program for multi-kinetic modeling of apatite fission-track data: Geological Materials Research, v. 2, p. 1–32, (*http://gmr.minsocam.org/papers/v2/2n1/v2n1abs.html*).

Klemperer, S. L., Hauge, T. A., Hauser, E. C., Oliver, J. E., and Potter, C. J., 1987, The Moho in the northern Basin and Range province along the COCORP 40°N seismic reflection transect: Geological Society of America Bulletin, v. 97, p. 603–618.

Laslett, G. M., Kendall, W. S., Gleadow, A. J. W., and Duddy, I. R., 1982, Bias in the measurements of fission-track length distributions: Nuclear Tracks and Radiation Measurements, v. 6, p. 79–85.

Lerch, D. W., Klemperer, S. L., Miller, E. L., and Colgan, J. P., 2005a, Velocity model from the 2004 Stanford University seismic experiment: a 260 km refraction/reflection/teleseismic survey in the northwestern Basin and Range: EarthScope National Meeting, Abstracts with Programs, p. 178.

Lerch, D., Colgan, J. P., Miller, E. L., and McWilliams, M. O., 2005b, Tectonic and magmatic evolution of the northwestern Basin and Range transition zone: Mapping and geochronology from the Black Rock Range, NV: Geological Society of America Abstracts with Programs, v. 37, n. 7, p. 70.

Ludwig, K. R., 2001, Squid: A users' manual: Berkeley Geochronology Center Special Publication 2, 19 p.

—— 2003, Isoplot 3.00, a geochronological tool-kit for Excel: Berkeley Geochronology Center Special Publication 4, 67 p.

McDowell, F. W., McIntosh, W. C., and Farley, K. A., 2005, A precise $^{40}Ar/^{39}Ar$ reference age for the Durango apatite (U-Th)/He and fission-track dating standard: Chemical Geology, v. 214, p. 249–263.

Meesters, A. G. C. A., and Dunai, T. J., 2002, Solving the production–diffusion equation for finite diffusion domains of various shapes: Part II. Application to cases with a-ejection and nonhomogeneous distribution of the source: Chemical Geology, v. 186, p. 347–363.

Miller, E. L., Dumitru, T. A., Brown, R. W., and Gans, P. B., 1999, Rapid Miocene slip on the Snake Range–Deep Creek Range fault system, east-central Nevada: Geological Society of America Bulletin, v. 111, p. 886–905.

Minor, S. A., ms, 1986, Stratigraphy and structure of the western Trout Creek and northern Bilk Creek Mountains, Harney County, Oregon, and Humboldt County, Nevada: Colorado, University of Colorado, M.S. thesis, 177 p.

Minor, S. A., and Wager, M., 1989, Geologic map of the Trident Peak SE quadrangle, Humboldt County, Nevada: U. S. Geological Survey Open-File Report 89–561, scale 1:24,000.

Minor, S. A., Wager, M., and Harwood, C. S., 1989, Geologic map of the Trident Peak SW quadrangle, Humboldt County, Nevada: U.S. Geological Survey Open-File Report 89–447, scale 1:24,000.

Mooney, W. D., and Weaver, C. S., 1989, Regional crustal structure and tectonics of the Pacific Coastal States; California, Oregon, and Washington, *in* Pakiser, L. C., and Mooney, W. D., editors, Geophysical Framework of the Continental United States: Boulder, Colorado, Geological Society of America Memoir 172, p. 129-161.

Nash, J. T., Utterback, W. C., and Trudel, W. S., 1995, Geology and geochemistry of Tertiary host rocks, Sleeper gold-silver deposit, Humboldt County, Nevada: U.S. Geological Survey Bulletin 2090, 63 p.

Nicholson, C., Sorlien, C. C., Atwater, T., Crowell, J. C., and Luyendyk, B. P., 1994, Microplate capture, rotation, of western Transverse Ranges, and initiation of the San Andreas transform as a low-angle fault system: Geology, v. 22, p. 491–495.

Noble, D. C., McKee, E. H., Smith, J. G., and Korringa, M. K., 1970, Stratigraphy and geochronology of Miocene volcanic rocks in northwestern Nevada: U. S. Geological Survey Professional Paper 700D, p. 23–32.

Personius, S. F., and Mahan, S. A., 2005, Unusually low rates of slip on the Santa Rosa Range fault zone, northern Nevada: Bulletin of the Seismological Society of America, v. 95, p. 319–333, doi:10.1785/0120040001.

Pierce, L. A., and Morgan, K. L., 1992, The track of the Yellowstone hotspot: Volcanism, faulting, and uplift, *in* Link, P. K., Kuntz, M. A., and Platt, L., editors, Regional geology of eastern Idaho and western Wyoming: Geological Society of America Memoir 179, p. 1–53.

Quinn, M. J., Wright, J. E., and Wyld, S. J., 1997, Happy Creek igneous complex and tectonic evolution of the early Mesozoic arc in the Jackson Mountains, Northwest Nevada: Geological Society of America Bulletin, v. 109, p. 461–482.

Reiners, P.W., Brady, R., Farley, K. A., Fryxell, J. E., Wernicke, B., and Lux, D., 2000, Helium and argon thermochronometry of the Gold Butte block, south Virgin Mountains, Nevada: Earth and Planetary Science Letters, v. 178, p. 315–326.

Reiners, P. W., Zhou, Z., Ehlers, T. A., Xu, C., Brandon, M. T., Donelick, R. A., and Nicolescu, S., 2003, Post-orogenic exhumation of the Dabie Shan, eastern China, from fission-track and (U-Th)/He thermochronology: American Journal of Science, v. 303, p. 489–518.

Roback, R. C., van der Meulen, D. B., King, H. D., Plouff, D., Munts, S. R., and Willet, S. L., 1987, Mineral Resources of the Pueblo Mountains Wilderness Study Area, Harney County, Oregon and Humbodlt County, Nevada: U.S. Geological Survey Bulletin 1740-B, p. B1–B30, scale: 1:48,000.

Rothstein, D. A., and Manning, C. E., 2003, Geothermal gradients in continental magmatic arcs: Constraints from the eastern Peninsular Ranges batholith: Geological Society of America Special Paper 374, p. 337–354.

Rytuba, J. J., and McKee, E. H., 1984, Peralkaline ash flow tuffs and calderas of the McDermitt volcanic field, southeast Oregon and north central Nevada: Journal of Geophysical Research, v. 89, p. 8616–8628.

Saleeby, J., Ducea, M., and Clemens-Knott, D., 2003, Production and loss of high density batholithic root, southern Sierra Nevada, California: Tectonics, v. 22, p. 1064, doi:10.1029/2002TC001374.

Saltus, R. W., and Jachens, R. C., 1995, Gravity and basin-depth maps of the Basin and Range province, western United States: U.S. Geological Survey Geophysical Investigations Map GP–1012, scale 1:2,500,000, 1 sheet.

Smith, D. L., 1992, History and kinematics of Cenozoic extension in the northern Toiyabe Range, Lander County, Nevada: Geological Society of America Bulletin, v. 104, p. 789–801.

Smith, D. L., Gans, P. B., Miller, E. L., Lisle, R. E., Schafer, R. W., and Wilkinson, W. H., 1991, Palinspastic restoration of Cenozoic extension in the central and eastern Basin and Range Province at latitude 39-40 degrees N, *in* Raines, G. L., Lisle, R. E., Schafer, R. W., and Wilkenson, W. H., editors, Geology and ore deposits of the Great Basin: Reno, Nevada, Geological Society of Nevada, p. 75–86.

Smith, J. G., McKee, E. H., Tatlock, D. B., and Marvin, R. F., 1971, Mesozoic granitic rocks in northwestern Nevada: A link between the Sierra Nevada and Idaho batholiths: Geological Society of America Bulletin, v. 82, p. 2933–2944.

Sonder, L. J., and Jones, C. H., 1999, Western United States extension: How the west was widened: Annual Review of Earth and Planetary Science Letters, v. 27, p. 416–472.

Stewart, J. H., and Carlson, J. E., 1978, Geologic map of Nevada: U. S. Geological Survey, scale 1:500,000.

Stockli, D. F., 2005, Application of low-temperature thermochronometry to extensional tectonic settings, *in* Reiners, P. W., and Ehlers, T. A., editors, Low-temperature thermochronology: Techniques, interpretations, and applications: Reviews in Mineralogy and Geochemistry, v. 58, p. 411–439.

Stockli, D. F., Linn, J. K., Walker, J. D., and Dumitru, T. A., 2001, Miocene unroofing of the Canyon Range during extension along the Sevier Desert Detachment, west-central Utah: Tectonics, v. 20, p. 289–307.

Stockli, D. F., Surpless, B. E., Dumitru, T. A., and Farley, K. A., 2002, Thermochronological constraints on the timing and magnitude of Miocene and Pliocene extension in the central Wassuk Range, western Nevada: Tectonics, v. 21, doi: 10.1029/2001TC001295.

Stockli, D. F., Dumitru, T. A., McWilliams, M. O., and Farley, K. A., 2003, Cenozoic tectonic evolution of the White Mountains, California and Nevada: Geological Society of America Bulletin, v. 115, p. 788–816.

Surpless, B. E., 2006, The Northwestern boundary of the Basin and Range Province: A structural study of the northern termination of the Warner Range, CA: Geological Society of America Abstracts with Programs, v. 38, p. 19.

Surpless, B. E., Stockli, D. F., Dumitru, T. A., and Miller, E. L., 2002, Two-phase westward encroachment of Basin and Range extension into the northern Sierra Nevada: Tectonics, v. 21(1), 1002, doi:10.1029/2000TC001257.

Tagami, T., and O'Sullivan, P. B., 2005, Fundamentals of fission-track thermochronology, *in* Reiners, P. W., and Ehlers, T. A., editors, Low-temperature thermochronology: Techniques, interpretations, and applications: Reviews in Mineralogy and Geochemistry, v. 58, p. 2-47.

Trexler, J. H., Cashman, P. H., Henry, C. D., Muntean, T., Schwartz, K., TenBrink, A., Faulds, J. E., Perkins, M., and Kelly, T., 2000, Neogene basins in western Nevada document the tectonic history of the Sierra Nevada – Basin and Range transition zone for the last 12 Ma, *in* Lageson, D. R., Peters, S. G., and Lahren, M. M., editors., Great Basin and Sierra Nevada: Boulder, Colorado, Geological Society of America Field Guide 2, p. 97–116.

Walker, G. W., and MacLeod, N. S., 1991, Geologic map of Oregon: U.S. Geological Survey Special Geologic Map, 2 sheets, scale 1:500,000.

Wernicke, B. P., and Snow, J. K., 1998, Cenozoic tectonism in the central Basin and Range: Motion of the Sierran-Great Valley Block: International Geology Review, v. 40, p. 403–410.

Whitehill, C. S., Miller, E. L., Colgan, J. P., Dumitru, T. A., Lerch, D. L., and McWilliams, M. O., 2004, Extent, style and age of Basin and Range faulting east of Pyramid Lake: Geological Society of America Abstracts with Programs, v. 36, n. 4, p. 37.

Wolak, C. E., ms, 2001, Mesozoic structure, stratigraphy, and magmatism in the eastern Pueblo Mountains, southeast Oregon and northwest Nevada: A record of an allochthonous arc terrane: University of Georgia, M.S. thesis, 180 p.

Wolf, R. A., Farley, K. A., and Kass, D. M., 1998, Modeling of the temperature sensitivity of the apatite (U-Th)/He thermochronometer: Chemical Geology, v. 148, p. 105–114.

Wolfe, J. A., Forest, C. E., and Molnar, P., 1998, Paleobotanical evidence of Eocene and Oligocene paleoaltitudes in midlatitude North America: Geological Society of America Bulletin, v. 110, p. 664–678.

Wyld, S. J., 1996, Early Jurassic deformation in the Pine Forest Range, northwest Nevada, and implications for Cordilleran tectonics: Tectonics, v. 15, p. 566–583.

—— 2002, Structural evolution of a Mesozoic backarc fold-and-thrust belt in the U.S. Cordillera: New evidence from northwestern Nevada: Geological Society of America Bulletin, v. 114, p. 1452–1486.

Wyld, S. J., and Wright, J. E., 2001, New evidence for Cretaceous strike-slip faulting in the United States Cordillera, and implications for terrane-displacement, deformation patterns, and plutonism: American Journal of Science, v. 301, p. 150–181.

Wyld, S. J., Rogers, J. W., and Copeland, P., 2003, Metamorphic evolution of the Luning-Fencemaker fold-thrust belt, Nevada: Illite crystallinity, metamorphic petrology, and ^{40}Ar/^{39}Ar geochronology: The Journal of Geology, v. 111, p. 17–38.

Zeitler, P. K., Herczeg, A. L., McDougall, I., and Honda, M., 1987, U-Th-He dating of apatite: A potential thermochronometer: Geochimica et Cosmochimica Acta, v. 51, p. 2865–2868.